Journal of Engineering Mathematics **50:** 177–208, 2004.

Wave dynamics on a thin-liquid film falling down a heated wall

PHILIP M.J. TREVELYAN and SERAFIM KALLIADASIS
Department of Chemical Engineering, University of Leeds, Leeds, LS2 9JT, UK; Current address: Department of Chemical Engineering, Imperial College London, London, SW7 2AZ, U.K.

Received 12 December 2003; accepted in revised form 26 June 2003

Abstract. The dynamics of a thin liquid film falling down a uniformly heated wall is studied. The model introduced by Kalliadasis *et al*. [J. Fluid Mech. 475 (2003) 377] for the same problem is revisited and its deficiencies, namely the prediction of a critical Reynolds number with 20% error, cured. For the energy equation a high-order Galerkin projection in terms of polynomial test functions is developed. It is shown that not only does this more refined formulation correct the critical Reynolds number, but it also gives, with an appropriate expansion close to criticality, the long-wave theory. Bifurcation diagrams for permanent solitary waves are constructed and compared with the solution branches obtained from different models. It is shown that, in all cases, the long-wave theory exhibits limit points and branch multiplicity, while the other models predict the continuing existence of solitary waves. Time-dependent computations show that the free surface and interfacial temperature approach a train of coherent structures that resemble the infinite-domain stationary solitary pulses.

Key words: falling film, solitary waves, thermocapillary Marangoni effect

1. Introduction

An isothermal film falling down a planar substrate exhibits a rich variety of spatial and temporal structures. It is a convectively unstable open-flow hydrodynamic system with a sequence of wave transitions that begins with amplification of small-amplitude white noise at the inlet, filtering of linear stability, secondary modulation instability that transforms the primary wave field into a solitary pulse and inelastic pulse-pulse interaction. This evolution is driven by the classical long-wave instability mode first observed in the pioneering experiments by Kapitza and Kapitza [1]. This mode was analyzed in detail by Benjamin [2] who determined its threshold and showed that a falling liquid film can only be destabilized with small but finite inertia.

During the last three decades, the falling-film problem has been the subject of intensive research by a large number of authors. The main advances include weakly nonlinear analyses leading to model partial-differential equations (Kuramoto-Sivashinsky and Ginsburg-Landau equations), strongly nonlinear analyses with construction of stationary periodic and solitary wave solutions and theory of stability of two-dimensional waves to both two- and three-dimensional disturbances as well as investigation of soliton-soliton and soliton-wave packet interaction. Detailed reviews of the main developments on falling film instabilities and related wave transitions are given in [3, 4].

The onset of the instability for a film falling down a uniformly heated wall was analyzed in detail by Goussis and Kelly [5]. In this case the wall heating generates a temperature distribution on the free surface which in turn induces surface-tension gradients that affect the free surface and therefore the fluid flow. Goussis and Kelly performed a linear stability

analysis based on Orr-Sommerfeld and linearized energy equations. They provided a detailed numerical solution of the pertinent eigenvalue problem and demonstrated that in addition to the Kapitza hydrodynamic mode of instability, the heated falling film is also subject to two thermocapillary instability modes: a short-wave mode obtained first by Scriven and Sternling [6] who considered the thermocapillary instability of an horizontal layer with a nondeformable free surface and a long-wave mode obtained first by Pearson [7] who allowed the free surface to deform.

The nonlinear stage of the instability for the heated falling film was investigated by Joo *et al.* [8] who utilized the usual long-wave lubrication approximation to obtain an evolution equation for the film thickness. In addition to Marangoni effects, they also included evaporation effects and long-range attractive intermolecular interactions. Joo *et al.* performed time-dependent computations of their evolution equation and observed a number of phenomena: wave breaking due to the surface-wave instability, thermocapillary instability which acts strongly on surface depressions, evaporative instability (vapour recoil) which causes the wave troughs to thin and finally film rupture. These authors also performed several numerical experiments which indicate finite-time blow-up behavior -referred to as 'super-exponential' or 'catastrophic' behavior by the authors.

A detailed investigation of the long-wave instabilities on the surface of a film falling down a uniformly heated wall was undertaken recently by Kalliadasis *et al.* [9]. Their analysis was based on the model equations derived by Kalliadasis *et al.* [10] in their study of the thermocapillary instability of a thin liquid film heated from below by a local heat source. We shall subsequently refer to these equations as the 'KKD model'. Its derivation was based on the integral-boundary-layer (IBL) approximation of the Navier-Stokes/energy equations and wall/free surface boundary conditions. For isothermal flows, this approach was introduced by Shkadov [11, 12] in two dimensions and Demekhin and Shkadov [13] in three dimensions. It combines the boundary-layer approximation of the Navier-Stokes equation assuming a self-similar velocity profile and long waves on the interface with the Kármán-Pohlhausen averaging method in boundary-layer theory. In two dimensions this approach results in a system of two coupled nonlinear partial differential equations for the evolution of the film thickness and flow rate in the streamwise direction. In the presence of thermal effects we have an additional equation for the interfacial temperature distribution.

Kalliadasis *et al.* [9] examined systematically the linear stability properties of the KKD model. In particular, they showed that the role of the Marangoni effect is to amplify the usual downstream propagating surface hydrodynamic mode of instability for an isothermal film and not to introduce a new unstable mode. The hydrodynamic mode is now characterized by an unusually large growth rate for very thin films. The neutral stability curves as a function of the relevant dimensionless groups, namely the Marangoni number, were found to be in qualitative agreement with those obtained by the Goussis and Kelly [5] classical Orr-Sommerfeld linear stability analysis. However, there was a difference between the neutral conditions obtained from the KKD IBL model and the original ones in the Goussis and Kelly Orr-Sommerfeld analysis with the maximum error introduced by KKD of the order of 20%. In addition, the critical Reynolds number obtained from the KKD model had a 20% error compared to the critical value obtained from Orr-Sommerfeld or the usual long-wave lubrication approximation – its important to note here that as was emphasized by Kalliadasis *et al.* [9] the long-wave expansion is exact close to criticality. A similar discrepancy for the critical Reynolds number predicted by IBL is also found for the isothermal falling film problem (see *e.g.* [4]).

Kalliadasis *et al.* also examined in detail the solitary wave solutions of the KKD model for both free surface and interfacial temperature. The solutions were contrasted with those obtained from the Joo *et al.* [8] long-wave model. The two approaches gave similar solitary wave solutions up to an $O(1)$ Reynolds number above which the solitary wave solution branch obtained by the Joo *et al.* equation is unrealistic with branch multiplicity and limit points. The IBL KKD approximation on the other hand has no limit points and predicts the continuing existence of solitary waves for all Reynolds numbers.

In this study we revisit the KKD model and we cure its deficiencies at the onset of the instability. For the isothermal falling-film problem, the IBL approximation was recently corrected by Ruyer-Quil and Manneville [14] who demonstrated that a simple Galerkin projection for the velocity field with just one test function (the self-similar parabolic profile assumed by Shkadov) and a weight function the test function itself, fully corrects the critical Reynolds number. We demonstrate here that a similar approach for the velocity field also recovers the correct critical Reynolds number for the problem of a film falling down a uniformly heated wall.

For the energy equation, on the other hand, we employ two different approaches: (i) we adopt the linear self-similar temperature distribution suggested by Kalliadasis *et al.* [9, 10]. The resulting energy equation along with the corrected momentum equation will be referred to as the 'improved KKD model'. The basic assumption for the distribution used in [9, 10] was that the linear temperature profile obtained for a flat film persists when the interface is no longer flat. However, this profile does not satisfy all boundary conditions for the temperature; (ii) a more refined formulation based on a high order Galerkin projection in terms of polynomial test functions. The temperature profile now satisfies all boundary conditions effectively through a 'tau' method [15].

This results in a set of nonlinear partial differential equations for the amplitudes of the temperature field coupled to the hydrodynamic equations for the film thickness and flow rate in the streamwise direction. We will be referring to this system as the 'TK1[m] model' where m is the number of modes for the temperature field.

We demonstrate that for this model a minimum of three amplitude equations for the temperature is necessary to obtain with an appropriate gradient expansion the long-wave theory close to criticality and hence to fully resolve the linear instability threshold. For the long-wave theory we assume a large Péclect number so that we can include the convective heat transport effects at a low relevant order. Hence, not only do we correct the critical Reynolds number but we also obtain the full long-wave lubrication approximation close to criticality (recall that in this regime the long-wave theory is exact).

We then construct numerically traveling-wave solutions of the solitary-wave type for both the free surface and the interfacial temperature. We shall demonstrate that our numerical analysis for the solitary waves is facilitated if the weight functions in the projection of the energy equation are appropriately modified. This new model will be referred to as the 'TK2[m] model' with m the number of modes for the temperature field. We contrast the solitary wave solutions of the large-Péclet number long-wave theory, the improved KKD and TK2[1] models. We obtain bifurcation diagrams for the speed and maximum amplitude of the solitary waves as a function of Reynolds number and for different values of the pertinent parameters, namely Marangoni and Prandtl numbers.

The bifurcation diagrams are qualitatively similar to those obtained by Kalliadasis *et al.* [9]: in all cases, the bifurcation diagrams for the large-Péclet-number long-wave theory exhibit limit points and multiplicity with two branches, a lower branch and an upper branch. This

lower branch and for small Reynolds numbers is in agreement with the other two models. The agreement persists up to an $O(1)$ Reynolds number above which the long-wave equation does not predict the existence of solitary waves. The two other models, however, predict the continuing existence of solitary waves for all Reynolds numbers.

Finally we perform time-dependent computations for the improved KKD model in the region of moderate Reynolds and Péclet numbers. We demonstrate that the final result of the evolution is a train of soliton-like coherent structures for both the free surface and the interfacial temperature which interact indefinitely with each other and which resemble the infinite-domain solitary pulses.

Our study should be relevant to a wide variety of technological applications. Indeed, thin liquid films are often encountered in heat-transport processes in engineering applications as a means to control fluxes and to protect surfaces: evaporators, condensers, heat exchangers and heat pipes, emergency cooling of nuclear fuel rods to name but a few. All these industrial processes involve heat transport from a hot wall to a film. The solitary waves on the surface of the film play a central role in these processes as they significantly enhance heat transport across the film.

The paper is organized as follows. In Section 2 we formulate the governing equations and we introduce the relevant dimensionless groups. In Section 3 we develop a long-wave theory for large Péclet numbers. The weighted residuals approach for the momentum equation is given in Section 4 while the weighted residuals approach and high-order Galerkin projection for the energy equation is given in Section 5. In Section 6 we construct numerically nonlinear solutions of the solitary wave type for the long-wave theory, improved KKD and TK2[1] models. In Section 7 we derive a model equation for small Reynolds numbers while in Section 8 we compare the different models to a finite-differences solution of the energy equation in two dimensions. In Section 9 we present time-dependent computations of the improved KKD model. Finally, a discussion and conclusions are given in Section 10.

2. Problem definition, scalings and governing equations

We consider a thin liquid film falling down a uniformly heated wall, as illustrated in Figure 1. The wall forms an angle θ with the horizontal direction. The liquid has viscosity μ, density ρ, constant pressure heat capacity c_p and thermal conductivity κ. The thermal conductivity of the solid substrate is assumed to be large so that it can be considered as a perfect heat conductor maintained at temperature T_w. The ambient gas phase is air maintained at temperature T_a. The liquid is assumed non-volatile so that evaporation effects can be neglected. It is also assumed sufficiently thin so that buoyancy effects are neglected. The heating provided by the wall induces a thermocapillary Marangoni effect at the interface which affects the interface and therefore the fluid flow.

The governing equations, namely continuity, Navier-Stokes and the energy equation are:

$$\underline{\nabla} \cdot \underline{u} = 0, \tag{1a}$$

$$\underline{u}_t + (\underline{u} \cdot \underline{\nabla})\underline{u} = -\frac{1}{\rho}\underline{\nabla} p + \nu \nabla^2 \underline{u} + \underline{g}, \tag{1b}$$

$$\rho c_p [T_t + (\underline{u} \cdot \underline{\nabla})T] = \kappa \nabla^2 T, \tag{1c}$$

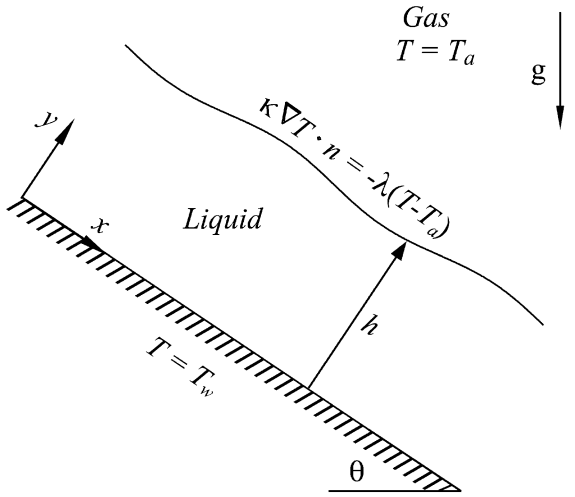

Figure 1. Sketch of the profile geometry for a thin liquid film falling down an inclined heated wall. The wall is maintained at temperature $T = T_w$ and forms an angle θ with the horizontal direction. The surrounding gas phase is maintained at temperature $T_a (< T_w)$. At the interface $y = h(x, t)$ the film looses heat according to Newton's law of cooling.

where $\underline{u}$, p and T are the velocity, pressure and temperature of the fluid, respectively. $\underline{g}$ is the gravitational acceleration and $\nu = \mu/\rho$ is the kinematic viscosity of the liquid. On the wall we have the usual boundary conditions for the velocity and temperature fields

$$\underline{u} = \underline{0}, \qquad T = T_w \tag{2}$$

while on the interface, $y = h(x, t)$, we have the usual normal and tangential stress balances, Newton's law of cooling and the kinematic boundary condition:

$$p_a + \underline{\underline{\tau}} \cdot \underline{n} \cdot \underline{n} = -\sigma \underline{\nabla} \cdot \underline{n}, \quad \underline{\underline{\tau}} \cdot \underline{n} \cdot \underline{t} = \underline{\nabla} \sigma \cdot \underline{t}, \quad \kappa \underline{\nabla} T \cdot \underline{n} = -\lambda (T - T_a), \quad h_t + u h_x = v \tag{3}$$

where p_a is the pressure of the ambient gas phase, σ is surface tension, $\underline{n}$ and $\underline{t}$ are unit normal and tangential vectors on the interface, $\underline{\underline{\tau}} = -p\underline{\underline{I}} + 2\mu \underline{\underline{e}}$ the stress tensor, $\underline{\underline{e}}$ the rate of strain tensor given by $e_{ij} = (\partial u_i/\partial x_j + \partial u_j/\partial x_i)/2$ and λ the heat-transfer coefficient describing the rate of heat transport from the liquid to the ambient gas phase.

The full system of Navier-Stokes/ energy equations and wall/free-surface boundary conditions has the trivial solution

$$h = h_0, \quad p = p_a + \rho(h_0 - y) g \cos\theta, \quad u = (2h_0 y - y^2) g \sin\theta / 2\nu, \quad v = 0,$$

$$T = T_w - y\lambda T_w / (h_0 \lambda + \kappa),$$

where u and v are the x- and y-components of the velocity, respectively. Hence the trivial solution is that of a flat film with a semi-parabolic velocity profile and a linear temperature decay. We utilize this trivial solution to introduce the non-dimensionalization

$$x \to \ell x, \quad (y, h) \to h_0 (y, h), \quad u \to u_0 u, \quad v \to \frac{h_0}{\ell} u_0 v, \quad t \to \frac{\ell}{u_0} t,$$

$$p \to p_a + \rho h_0 p g \sin\theta, \quad T \to T_a + T(T_w - T_a),$$

where $u_0 = h_0^2 g \sin\theta/2\nu$ is the interfacial velocity of the flat film (Nusselt velocity) and ℓ a characteristic lengthscale in the streamwise direction. Temperature scales with $T_w - T_a$ which would be the control variable in an actual experiment and time scales with ℓ/u_0, the time an interfacial fluid particle transverses a distance ℓ.

In terms of these non-dimensional variables, the equations of motion and energy become

$$u_x + v_y = 0, \tag{4a}$$

$$u_{yy} + 2 = 2\epsilon p_x + \epsilon \mathrm{Re}(u_t + uu_x + vu_y) - \epsilon^2 u_{xx}, \tag{4b}$$

$$\epsilon v_{yy} - 2\cot\theta = 2p_y + \epsilon^2 \mathrm{Re}(v_t + uv_x + vv_y) - \epsilon^3 v_{xx}, \tag{4c}$$

$$T_{yy} = \epsilon \mathrm{Pe}(T_t + uT_x + vT_y) - \epsilon^2 T_{xx}, \tag{4d}$$

where $\epsilon = h_0/\ell$ the film parameter, $\mathrm{Re} = u_0 h_0/\nu$ the Reynolds number and $\mathrm{Pe} = \mathrm{RePr}$ the Péclet number with $\mathrm{Pr} = \rho c_p \nu/\kappa$ the Prandtl number. The thermocapillary effect is modelled by using a linear approximation for the surface ension as a function of temperature,

$$\sigma = \sigma_0 - \gamma(T - T_0)$$

with σ_0 the surface tension at the reference temperature T_0 and $\gamma > 0$ for typical liquids. With this approximation and using the above non-dimensionalization, the boundary conditions at $y = h(x, t)$ in Equation (3) become

$$p = -\epsilon^2(\mathrm{We} - \mathrm{Ma}T)N^{-\frac{3}{2}} h_{xx} + \epsilon N^{-1}(v_y - h_x u_y + \epsilon^2(h_x^2 u_x - h_x v_x)) \tag{5a}$$

$$u_y + \epsilon^2(v_x + 2h_x(v_y - u_x) - h_x^2 u_y) - \epsilon^4 h_x^2 v_x = -2\epsilon \mathrm{Ma}(T_x + h_x T_y)N^{\frac{1}{2}} \tag{5b}$$

$$(T_y - \epsilon^2 h_x T_x)N^{-\frac{1}{2}} = -\mathrm{Bi}T \tag{5c}$$

$$h_t + uh_x = v \tag{5d}$$

where $N = 1 + \epsilon^2 h_x^2$, $\mathrm{Ma} = \gamma(T_w - T_a)/\rho h_0^2 g \sin\theta$ is the Marangoni number, $\mathrm{We} = \sigma_0/\rho h_0^2 g \sin\theta$ is the Weber number, and $\mathrm{Bi} = \lambda h_0/\kappa$ is the Biot number. Finally, the wall boundary conditions become

$$u = v = 0, \quad T = 1 \tag{5e}$$

Equations (4) and (5) are the basic equations for the analysis to follow. Our system is governed by five dimensionless groups: Re, We, Ma, Pr and Bi. Hence, a complete investigation over the entire parameter space would be an impossible task. However, as was pointed out by Kalliadasis *et al.* [9], we can reduce the number of relevant dimensionless groups by fixing the liquid and expressing our groups in terms of parameters which depend only on the physical properties of the liquid. We then introduce

$$\chi = \frac{gh_0^3}{\nu^2}, \quad \mathrm{Ka} = \frac{\sigma_0}{\rho\nu^{4/3}g^{1/3}}, \quad M = \frac{\gamma(T_w - T_a)}{\rho\nu^{4/3}g^{1/3}}, \quad B = \frac{\lambda\nu^{2/3}}{\kappa g^{1/3}},$$

where χ, M and B are the *modified* Reynolds, Marangoni and Biot numbers, respectively and Ka is the Kapitza number. We then have

$$\mathrm{Re} = \frac{\chi}{2}\sin\theta, \quad \mathrm{We} = \frac{\mathrm{Ka}}{\chi^{2/3}\sin\theta}, \mathrm{Ma} = \frac{M}{\chi^{2/3}\sin\theta}, \ \mathrm{Bi} = B\chi^{1/3}.$$

Notice now that the introduction of χ isolates the θ dependence of the Reynolds number. Notice also that Ka, M and B are independent of h_0 which is a flow control parameter and depend only on the physical properties of the liquid phase, the heat-transfer coefficient of the liquid-gas interface and the temperature difference $T_w - T_a$. Hence, for a given-liquid gas system, the only relevant parameters are χ, M and θ while the vertical heated falling film problem is a two-parameter system only. If the liquid phase is water at 25 °C, Ka $\simeq$ 2850 and Pr $\simeq$ 7. It is also realistic to expect the gas to be a poor conductor and so the parameter B should be small. For convenience we shall fix Ka = 3000 and in the absence of experimental values for Biot numbers of liquid-gas interfaces we take $B = 0{\cdot}1$ throughout this study.

3. Long-wave theory for large Péclet numbers

The complexity of the free-boundary problem in Equations (4) and (5) can be removed by invoking a long-wave (lubrication) expansion for $\epsilon \ll 1$. This allows an asymptotic reduction of the governing equations and boundary conditions to a single nonlinear partial differential equation of the evolution type formulated in terms of the local film thickness (see [16] for a detailed review of long-wave theories). In the presence of Marangoni effects one typically assumes Pe = $O(1)$ and expands u up to $O(\epsilon)$ and T up to $O(1)$. As a consequence the convective heat transport effects are not retained. To include these effects one would have to expand u up to $O(\epsilon^2)$ and T up to $O(\epsilon)$ but these higher order corrections are rather lengthy.

Experiments for the problem of a falling film heated from below by a local heat source [17], indicate that the Péclet number can be large. We expect that convection at large Péclet numbers can lead to a downstream convective distortion of the free-surface temperature distribution obtained by assuming an $O(1)$ Péclet number. Here we assume the Péclet number to be large so that the convective heat transport effects are included at a lower relevant order. More specifically we take Pe = $O(\epsilon^{-n})$ for $0 < n < 1$. We also assume Re = $O(1)$, We = $O(\epsilon^{-2})$, Ma = $O(1)$ and Bi = $O(1)$.

We then carry out an expansion in ϵ up to $O(\epsilon^{2-n})$ and we neglect terms of $O(\epsilon^2)$ and higher. This level of truncation allows the derivation of a relatively simple evolution equation for the free surface as the $O(\epsilon^2)$ terms are rather lengthy. The pressure and temperature field are both expanded up to $O(\epsilon^{1-n})$ and hence terms of $O(\epsilon)$ and higher are omitted in these expansions. At this level of truncation, the pressure is given by

$$p = \cot\theta(h - y) - \epsilon^2 \mathrm{We} h_{xx} \tag{6}$$

and the temperature field by

$$\begin{aligned} T \;=\; & 1 - \frac{\mathrm{Bi}y}{1+\mathrm{Bi}h} - \frac{\epsilon \mathrm{PeBi}h_x y^3}{60(1+\mathrm{Bi}h)^2}(3\mathrm{Bi}y^2 - (5+15\mathrm{Bi}h)y + 20\mathrm{Bi}h^2) \\ & - \frac{\epsilon \mathrm{PeBi}h^3 h_x y}{30(1+\mathrm{Bi}h)^3}(10 - 5\mathrm{Bi}h - 4\mathrm{Bi}^2h^2) \end{aligned} \tag{7}$$

Details of the derivation are given in Appendix 1. The velocity components are given by $u = \psi_y$ and $v = -\psi_x$ where the stream function ψ is found to be

$$\begin{aligned} \psi \;=\; & y^2\left(h - \frac{y}{3}\right)(1 + \epsilon^2 \mathrm{We} h_{xxx} - \epsilon h_x \cot\theta) + \epsilon h h_x y^2 \frac{\mathrm{Re}}{30}(20h^3 - 5hy^2 + y^3) \\ & + \epsilon \frac{\mathrm{MaBi}y^2}{(1+\mathrm{Bi}h)^2} h_x + \epsilon^2 \mathrm{PeMaBi}y^2 \left(\frac{(15 - 7\mathrm{Bi}h)h^4 h_x}{60(1+\mathrm{Bi}h)^3}\right)_x . \end{aligned} \tag{8}$$

The free-surface evolution equation can then be easily obtained from the kinematic boundary condition in (5d):

$$h_t + 2h^2 h_x + \epsilon\left[\frac{8}{15}\mathrm{Re}h^6 h_x - \frac{2}{3}h^3 h_x \cot\theta + \frac{\mathrm{MaBi}h^2 h_x}{(1+\mathrm{Bi}h)^2} + \frac{2}{3}\epsilon^2 \mathrm{We}h^3 h_{xxx}\right]_x + \epsilon^2 \mathrm{PeMaBi}\left[h^2\left(\frac{(15-7\mathrm{Bi}h)h^4 h_x}{60(1+\mathrm{Bi}h)^3}\right)_x\right]_x = 0. \tag{9}$$

The second term in this equation is the convective term due to mean flow, the third term is due to inertia, the fourth term is due to the hydrostatic head in the direction perpendicular to the substrate, the fifth term is due to the Marangoni effect, the sixth term is the usual streamwise curvature gradient associated with surface tension and the seventh term originates from the heat-transport convective terms. The first two terms are $O(1)$, the third, fourth, fifth and sixth terms are $O(\epsilon)$ and the seventh term is of $O(\epsilon^{2-n})$. It is important to emphasize that in the absence of Marangoni effects, our free-surface evolution equation in (9) reduces to the $O(\epsilon)$ evolution equation that has been derived and studied by a number of authors (see *e.g.* [16]), Notice also that without the last term due to the convective heat transport effects, (9) is identical to the Joo *et al.* [8] evolution equation (in the absence of the additional effects due to evaporation and intermolecular forces considered by these authors),

It is now convenient to rescale the space and time coordinates as $x = \epsilon \mathrm{Re}^{1/3} X$ and $t = \epsilon \mathrm{We}^{1/3}\Theta$ which yields

$$h_\Theta + 2h^2 h_X + \frac{2}{3}\left[h^3(\mathcal{A}(h)h_X + \mathcal{B}(h)h_X^2 + \mathcal{C}(h)h_{XX} + h_{XXX})\right]_X = 0, \tag{10}$$

where $\mathcal{A}(h) = \mathrm{We}^{-1/3}(\frac{4}{5}\mathrm{Re}h^3 - \cot\theta + \frac{3}{2}\mathrm{Ma\,Bi}/h(1+\mathrm{Bi}h)^2)$, $\mathcal{B}(h) = \mathrm{We}^{-2/3}\mathrm{Ma\,BiPe}h^2(30 - 10\mathrm{Bi}h - 7\mathrm{Bi}^2h^2)/20(1+\mathrm{Bi}h)^4$ and $\mathcal{C}(h) = \mathrm{We}^{-2/3}\mathrm{Ma\,BiPe}h^3(15-7\mathrm{Bi}h)/40(1+\mathrm{Bi}h)^3$. We shall refer to this model equation obtained from a long-wave expansion as the 'LWE model'. Notice that the requirements on the order of magnitude of our dimensionless parameters imply that $\mathcal{A} \sim \epsilon^{2/3}$, and $\mathcal{B} \sim \mathcal{C} \sim \epsilon^{4/3-n}$. Recalling the requirement $0 < n < 1$ for our long-wave expansion, we obtain $\epsilon^{4/3} \ll \mathcal{B}, \mathcal{C} \ll \epsilon^{1/3}$. Therefore, the relative size between $\mathcal{A}$ and $\mathcal{B}$, $\mathcal{C}$ can only be determined when we assign a specific value for n. For instance, the value $n = 2/3$ yields the distinguished limit $\mathcal{A} \sim \mathcal{B} \sim \mathcal{C} \sim \epsilon^{2/3}$ showing that the convective effects can be equally important as inertia, hydrostatic head, capillary forces and Marangoni effects.

3.1. Linear stability of trivial solution

We now consider the stability of the trivial solution to infinitesimal perturbations in the form of the normal mode $h \sim 1 + \hat{h}\exp(\lambda\Theta + \mathrm{i}kX)$ which when substituted into the evolution equation in (10) and linearizing for $\hat{h} \ll 1$ yields

$$\lambda_R = \frac{2}{3}k^2(\overline{\mathcal{A}} - k^2), \tag{11a}$$

$$\lambda_I = -2k + \frac{2}{3}\overline{\mathcal{C}}k^3 \tag{11b}$$

for the real and imaginary parts of the growth rate λ as a function of wavenumber k, with $\overline{\mathcal{A}} \equiv \mathcal{A}(1)$ and $\overline{\mathcal{C}} \equiv \mathcal{C}(1)$. Hence, the normal modes on the flat film $h = 1$ represent infinitesimal disturbances traveling downstream with a velocity $-\lambda_I/k = 2 - (2/3)\overline{\mathcal{C}}k^2$.

The real part of λ indicates that the onset of instability occurs at $\overline{\mathcal{A}} = 0$ which yields the critical Reynolds number

$$\mathrm{Re}_c = \frac{5}{4}\cot\theta - \frac{15\mathrm{Ma}\,\mathrm{Bi}}{8(1+\mathrm{Bi})^2} \tag{12}$$

while the maximum growing linear mode at criticality, has a wavenumber that is exactly zero. Beyond onset, the neutral Wavenumber k_0 with zero growth rate occurs at $k = 0$ and at $k_c = \mathcal{A}^{1/2}$ and hence LWE predicts two branches of the neutral curve. The dispersion curve for the growth rate λ_R as a function of k is characterized by an unstable band $0 \leq k \leq k_c$ containing the maximum growing wavenumber $k_{\max} = (1/\sqrt{2})k_c$ with the largest growth rate.

The critical condition in (12) indicates that increasing Ma (with $\mathrm{Ma} > 0$) decreases Re_c and hence the Marangoni effect is destabilizing (stabilizing for $\mathrm{Ma} < 0$). For $\mathrm{Ma} = 0$ the condition is identical to that obtained by Benjamin [2] while for $\mathrm{Ma} \neq 0$ is exactly the same with the critical condition obtained in the Goussis and Kelly [5] linear stability analysis based on Orr-Sommerfeld and linearized energy equations. This is not surprising as LWE being a regular perturbation expansion of the full Navier-Stokes should be exact close to criticality (see also our discussion in the Introduction). Notice, however, that LWE predicts one mode only, as opposed to three modes (downstream propagating surface mode, upstream propagating surface and downstream propagating Marangoni modes) obtained from the KKD model in [9]. Moreover, LWE predicts two branches of the neutral curve for an inclined film, while the study by Kalliadasis *et al.* [9] clearly indicates the existence of three neutral curves. On the other hand, for sufficiently large M, Goussis and Kelly [5] obtain an additional neutral curve associated with the formation of rolls below the interface. However, convective cells and rolls cannot be captured by the KKD model and any IBL model for that matter since all these models ignore the viscous terms in the streamwise direction compared to the viscous terms in the direction perpendicular to the wall; see discussion in [9].

The long-wave expansion was developed to check that the integral-boundary-layer models developed in the following sections provide the correct behaviour close to criticality. It is also because of the presence of the convective heat transport terms in the integral-boundary-layer models that we develop a long-wave theory to include these terms.

4. Weighted residuals approach: momentum equation

As we have already emphasized in the Introduction, despite its good performance in the nonlinear regime, the KKD model predicts the critical condition with a 20% error. The aim here is not only to cure this discrepancy for the critical condition, but also develop higher order models that will give, with an appropriate expansion close to criticality, the full long-wave theory of the previous section.

The starting point of our analysis is to assume long waves in the streamwise direction and neglect the second-order diffusive terms u_{xx} and T_{xx} of the Navier-Stokes/energy equations. This assumption was also made by Kalliadasis *et al.* [10] and is effectively a boundary-layer approximation of the Navier-Stokes/energy equations. Part of our analysis at the beginning of this section parallels the works in [9, 10] and the reader is referred to these studies for further details.

To leading order, the y-component of the equation of motion (4c) and normal stress balance (5a) are $p_y = -\cot\theta$ and $p = -\epsilon^2 \mathrm{We} h_{xx}$ on $y = h(x,t)$. Hence, we obtain the same leading-

order pressure distribution as in Equation (6). Substituting now the expression for the pressure in the x-component of the momentum equation (4b) and neglecting terms of $O(\epsilon^2)$ and higher, we have

$$u_{yy} + 2 = 2\epsilon h_x \cot\theta - 2\epsilon^3 \mathrm{We} h_{xxx} + \epsilon \mathrm{Re}(u_t + uu_x + vu_y) \tag{13}$$

subject to the no-slip boundary conditions in (5e) and the leading. order tangential stress balance on the interface from (5b)

$$u_y = -2\epsilon \mathrm{Ma} \tau_x \quad \text{on} \quad y = h, \tag{14}$$

where terms of $O(\epsilon^2)$ and higher have been neglected and $\tau(x, t)$ denotes the free-surface temperature distribution, *i.e.*, $\tau \equiv T|_{y=h}$ and $\tau_x \equiv (T_x + h_x T_y)|_{y=h}$.

Following Kalliadasis *et al.* [9, 10] we assume that the velocity profile beneath the film has the self-similar form

$$u = 3\frac{q}{h}\left(\eta - \frac{1}{2}\eta^2\right) + \epsilon \mathrm{Ma} \tau_x h \left(\eta - \frac{3}{2}\eta^2\right), \tag{15}$$

where

$$\eta = \frac{y}{h(x,t)} \quad \text{and} \quad q = \int_0^h u \mathrm{d}y \tag{16}$$

is the flow rate in the streamwise direction. The continuity equation in (4a) along with the no slip condition, can be easily used to obtain v, $v = \int_0^y u_x \mathrm{d}y'$. For $\mathrm{Ma} = 0$, (15) is the profile introduced by Shkadov [11, 12]. Note that with the introduction of the flow rate q, the kinematic boundary condition in (5d) can be written as

$$h_t + q_x = 0. \tag{17}$$

The velocity distribution for u in (15) is the simplest possible profile which satisfies all boundary conditions. We also note that this profile trivially satisfies the x-component of the equation of motion at zero Reynolds and Marangoni numbers with $q = 2h^3/3$.

For the isothermal falling-film problem, Ruyer-Quil and Manneville [14] developed high-order IBL models using refined polynomial expansions for the velocity field (corresponding to corrections of the Shkadov self-similar profile) and high-order weighted residual techniques; the introduction of a test function for the velocity leads to a residual for the momentum equation. In our case, the introduction of the test function (15) yields the following residual for the x-component of the momentum Equation (13):

$$R_u = \epsilon \mathrm{Re}(u_t^{(0)} + u^{(0)}u_x^{(0)} + v^{(0)}u_y^{(0)}) - u_{yy} - 2 + 2\epsilon \cot\theta - 2\epsilon^3 \mathrm{We} h_{xxx}, \tag{18}$$

where $u^{(0)}$ and $v^{(0)}$ denote the leading-order terms from u and v with $v^{(0)} = \int_0^y u_x^{(0)} \mathrm{d}y'$, since the Marangoni terms in (15) are of $O(\epsilon \mathrm{Ma})$ (due to the long-wave approximation) so that they only contribute to the viscous-diffusion term $\partial^2/\partial y^2$ and are neglected in the inertial/convective terms which are of $O(\epsilon \mathrm{Re})$. Following the study by Ruyer-Quil and Manneville [14] for the isothermal film, the momentum residual can be minimized via a weighted residual approach that would yield a constraint on q and hence a closure for the system:

$$< w_u, R_u >= 0, \tag{19}$$

where w_u is the weight function and the inner product is defined as $< f, g >= \int_0^1 fg\mathrm{d}\eta$ for any two functions f and g with appropriate boundary conditions.

Specifying the weight function fixes the particular weighted-residual method being used. For the isothermal falling-film problem, Ruyer-Quil and Manneville [14] showed that the Kármán-Pohlhausen averaging method employed by Shkadov [11, 12] can be viewed as a special weighted-residual method with $w_u \equiv 1$. The same weight function was also adopted by Kalliadasis *et al.* [10] in the presence of thermal effects. The inner product $< 1, R_u >= 0$ then yields

$$\epsilon\mathrm{Re}\left(q_t + \frac{6}{5}\left(\frac{q^2}{h}\right)_x\right) + \frac{3q}{h^2} = 2h + 2\epsilon^3\mathrm{We}hh_{xxx} - 2\epsilon hh_x\cot\theta - 3\epsilon\mathrm{Ma}\tau_x \tag{20}$$

which is an evolution equation for q that involves the interfacial temperature τ which is unknown at this point.

For the isothermal falling-film problem, Ruyer-Quil and Manneville [14] showed that a Galerkin projection for the velocity field with just one test function (the self-similar profile assumed by Shkadov [11, 12]) and with the weight function as the test function itself fully corrects the critical Reynolds number obtained from the Shkadov IBL approximation. We shall demonstrate that this is also the case in the presence of Marangoni effects, in fact it is only necessary to take the weight function as the leading-order test function for the velocity, namely $w_u \equiv \eta - \frac{1}{2}\eta^2$. Substituting this in (19) and retaining only the dominant terms, we have

$$\frac{6}{5}\epsilon Re\left(q_t + \frac{17q}{7h}q_x - \frac{9q^2}{7h^2}h_x\right) + \frac{3q}{h^2} = 2h + 2\epsilon^3\mathrm{We}hh_{xxx} - 2\epsilon hh_x\cot\theta - 3\epsilon\mathrm{Ma}\tau_x \tag{21}$$

which is the momentum equation used in the remainder of this study.

5. Weighted-residuals approach: energy equation

The boundary conditions for the temperature field are the wall condition in (5e) and the leading-order Newton's law of cooling in (5c)

$$T_y = -\mathrm{Bi}T \quad \text{on} \quad y = h \tag{22}$$

where terms of $O(\epsilon^2)$ and higher have been neglected. Like the momentum equation, the first step for the energy equation would be the introduction of a self-similar profile. Kalliadasis *et al.* [9] equivalently assumed the distribution

$$T = 1 + (\tau - 1)\eta. \tag{23}$$

By analogy with our analysis in the previous section, the introduction of a test function for the temperature field yields a residual for the energy equation at $O(\epsilon)$

$$R_T = \epsilon\mathrm{Pe}(T_t + u^{(0)}T_x + v^{(0)}T_y) - T_{yy}, \tag{24}$$

where again the $O(\epsilon\mathrm{Ma})$ terms of u and v contribute only to the thermal diffusion term $\partial^2/\partial y^2$ and are neglected in the inertial/convective terms which are of $O(\epsilon\mathrm{Pe})$. The energy residual can then be minimized from

$$< w_T, R_T >= 0 \tag{25}$$

where w_T is an appropriately chosen weight function.

The temperature distribution in (23) satisfies the wall boundary condition in (5e) but does *not* satisfy the interfacial condition in (22) unlike the velocity profile in (15) which satisfies all boundary conditions. However, as was pointed out in [9], by choosing $w_T \equiv \eta$, the boundary terms resulting from integrations by parts involve either T_η on $\eta = 1$ or T on $\eta = 0$. Thus, we apply the boundary conditions prior to substituting the linear approximation in (23). Hence, although (23) does not satisfy all boundary conditions, the averaged energy equation does. The result is

$$\tau_t + \frac{27q}{20h}\tau_x + \frac{7q_x(\tau - 1)}{40h} + \frac{3}{\epsilon \mathrm{Pe} h^2}(\tau(\mathrm{Bi}h + 1) - 1) = 0 \tag{26}$$

Equations (20) and (26) along with the kinematic boundary condition in (17) constitute what we referred to in the Introduction as the KKD model while Equations (21), (26) and (17) constitute what we referred to in the Introduction as the improved KKD model.

As we have already emphasized, the improved KKD model fully corrects the critical Reynolds number obtained from the KKD model. However, we also wish to be able to obtain close to criticality the long-wave theory in Section 3. For this purpose a more refined treatment of the temperature field is required. We then project the temperature field onto the set of polynomial test functions

$$T(x, t, \eta) = \sum_{i=0}^{m+2} A^{(i-2)}(x, t)\eta^i,$$

where $A^{(j)}$ are the amplitudes of the expansion and m is an integer. The wall boundary condition $T = 1$ on $\eta = 0$ requires $A^{(-2)} = 1$. A Taylor-series expansion at $y = 0$ of the energy equation in (4d) then shows that $A^{(0)} = 0$ independently of the boundary conditions on the free surface. This is also consistent with our long-wave theory in Section 3. Notice also that unlike the isothermal film study by Ruyer-Quil and Manneville [14] where the amplitudes of the polynomial expansion for the velocity field are assigned certain orders with respect to the long-wave parameter ϵ, in our expansion for the temperature field the order of the amplitudes is not specified.

Substituting the polynomial expansion for the temperature field in boundary condition (22) or $T_\eta = -\mathrm{Bi}hT$ on $\eta = 1$ to eliminate $A^{(-1)}$, using $A^{(-2)} = 1$, $A^{(0)} = 0$ and eliminating $A^{(1)}$ from the definition $\tau \equiv T|_{n=1}$ defines a projection onto the new set of test functions ϕ_i,

$$T = \phi_0 + \tau\phi_1 + \sum_{i=2}^{m} A^{(i)}\phi_i, \tag{27}$$

where $\phi_0 = 1 - 3\eta/2 + \eta^3/2$, $\phi_1 = (\mathrm{Bi}h + 3)\eta/2 - (\mathrm{Bi}h + 1)\eta^3/2$ and $\phi_i = (i - 1)\eta/2 - (i + 1)\eta^3/2 + \eta^{i+2}$. Thus ϕ_0(0)-1 = $\phi_0(1) = \phi_{0_\eta}(1) = 0$, $\phi_1(0) = \phi_1(1) - 1 = \phi_{1_\eta}(1) + \mathrm{Bi}h = 0$ and for $i \geq 2$ we have $\phi_i(0) = \phi_i(1) = \phi_{i_\eta}(1) = 0$. Hence, we have introduced τ explicitly into our expansion and at the same time T satisfies Newton's law of cooling (unlike the simple expression in Equation (23)). In weighted-residuals terminology this is effectively a 'tau' method [15]. Note also that all the ϕ_i's are non-negative inside the open interval (0, 1).

We now let w_j denote our weight functions for the energy equation. The dominant terms from the residuals $< w_j, R_T > = 0$ are then denoted by r_j and are given by

$$r_j = \epsilon \mathrm{Pe}\left(\alpha_{1j}\tau_t + \beta_{1j}\tau_x + \gamma_{1j}\tau + \delta_j + \sum_{i=2}^{m} \alpha_{ij}A_t^{(i)} + \beta_{ij}A_x^{(i)} + \gamma_{ij}A^{(i)}\right) - \Delta_j - \Gamma_{1j}\tau - \sum_{i=2}^{m} \Gamma_{ij}A^{(i)}, \tag{28}$$

where $\alpha_{ij} =< w_j, \phi_i >$, $\beta_{ij} =< w_j, u^{(0)}\phi_i >$, $\gamma_{ij} =< w_j, \phi_{i_t} + u^{(0)}\phi_{i_x} + v^{(0)}\phi_{i_y} >$, $\delta_j =< w_j, \phi_{0_t} + u^{(0)}\phi_{0_x} + v^{(0)}\phi_{0_y} >$, $\Delta_j =< w_j, \phi_{0_{yy}} >$, and $\Gamma_{ij} =< w_j, \phi_{i_{yy}} >$.

At this point it is convenient to use matrix notation, and so by introducing $\underline{A} = [\tau, A^{(2)} \cdots A^{(m)}]^t$ we have

$$\epsilon \mathrm{Pe}\left(\underline{\underline{M_\alpha}}\ \underline{A}_t + \underline{\underline{M_\beta}}\ \underline{A}_x + \underline{\underline{M_\gamma}} + \underline{A} + \underline{\delta}\right) = \underline{\Delta} + \underline{\underline{M_\Gamma}}\underline{A} \tag{29}$$

where the matrices $[\underline{\underline{M_\alpha}}]_{ij} = \alpha_{ij}$, $[\underline{\underline{M_\beta}}]_{ij} = \beta_{ij}$, $[\underline{\underline{M_\gamma}}]_{ij} = \gamma_{ij}$ and $[\underline{\underline{M_\Gamma}}]_{ij} = \Gamma_{ij}$ are of dimension $m \times m$ and the vectors $[\underline{\delta}]_j = \delta_j$ and $[\underline{\Delta}]_j = \Delta_j$ are of dimension $m \times 1$.

5.1. Galerkin projection for the energy equation

We take the weight functions in Equation (29) to be the same as the test functions in (27), *i.e.*, $w_j \equiv \phi_j$. This is then a Galerkin projection in weighted-residuals terminology. We now demonstrate that the LWE model of Section 3 can be obtained with an appropriate expansion of the system in (29). For this purpose we assign for Re, Pe, We, Ma and Bi the same orders of magnitude with LWE. It is important to point out here that our averaged model in (29) has been derived without overly restrictive stipulations on the order of the dimensionless groups (see [9,10] for a discussion of lower/upper bounds on the order of magnitude of the dimensionless parameters). For example, changing the order of Pe in (29) would lead to a different long-wave expansion to that obtained in Section 3.

Let us now expand q and the amplitudes τ and $A^{(i)}$ as $q = q^0 + \epsilon q^1 + O(\epsilon^2)$, $\tau = \tau_0 + \epsilon^{1-n}\tau_1$, $A^{(i)} = A_{0i} + \epsilon^{1-n}A_{1i}$ where $\mathrm{Pe} = O(\epsilon^{-n})$ with $0 < n < 1$ and we truncate our expansions so that terms of $O(\epsilon^2)$ and higher in (21) are neglected while terms of $O(\epsilon)$ and higher in (29) are neglected. Equation (21) then yields

$$q = \frac{2}{3}h^3 + \frac{15}{8}\epsilon \mathrm{Re}h^6 h_x - \frac{2}{3}h^3 h_x \cot\theta - \epsilon \mathrm{Ma}h^2\tau_x + \frac{2}{3}\epsilon^3 \mathrm{We}h^3 h_{xxx}, \tag{30}$$

which is identical to the flow rate obtained from LWE. We note that at this point τ_x from the averaged system in (29) remains undetermined, however, we shall demonstrate that it is exactly the same with the one obtained from LWE.

The reason why Equation (21) corrects the critical condition is that Re_c originates from the inertia and Marangoni terms in the expression for the flow rate in (30). The inertia coefficient in (30) is 15/8, *i.e.* exactly the same with LWE while a linear stability analysis shows that the convective terms of the energy equation do not contribute to the critical condition (this is effectively the reason why (12) is independent of Pr). Hence, it is always the term $1/(1 + \mathrm{Bi}h)$ obtained from the interfacial temperature distribution in the absence of convective effects, *i.e.*, for $\epsilon\mathrm{Pe} = 0$ that contributes to Re_c. Since all temperature profiles including the linear profile in (23) give $1/(1 + \mathrm{Bi}h)$ in the absence of convective effects (see Equation (26)), (21) and

Table 1. Summary of equations for the different time-dependent models. m is the number of modes for the temperature field.

LWE	KKD	Improved KKD	TK1[m]
	(17)	(17)	(17)
(10)	(20)	(21)	(21)
	(26)	(26)	(29) with $w_i = \phi_i$

therefore (30) predicts the same Re_c with (12). On the other hand, a linear stability analysis of (20) and (23) (effectively the KKD model) would give for Re_c the same functional form with (12) but with a coefficient of 1 instead of 5/4 in front of $\cot\theta$.

Substituting now q from Equation (30) in Equation (29), the ϵ^{1-n}-expansions for the temperature and utilizing the kinematic boundary condition we obtain

$$\tau = \frac{1}{1+\mathrm{Bi}h} + \epsilon\mathrm{PeBi}h^4 h_x \frac{7\mathrm{Bi}h - 15}{60(1+\mathrm{Bi}h)^3},$$

$$A^{(2)} = \epsilon\mathrm{PeBi}h^4 h_x \frac{3\mathrm{Bi}h + 1}{12(1+\mathrm{Bi}h)^2}, \quad A^{(3)} = -\frac{\epsilon\mathrm{PeBi}^2 h^5 h_x}{20(1+\mathrm{Bi}h)^2}$$

with $A^{(i)} = 0$ for $i \geq 4$. When these expressions are substituted in Equation (27) they yield Equation (7). Hence, we obtain the same interfacial temperature distribution leading to the same long-wave expansion with Section 3.

Since now in order to obtain the long-wave theory of Section 3 from an appropriate expansion of our Galerkin system we need $m \geq 3$ to $O(\epsilon\mathrm{Pe})$, we truncate our temperature expansion at $m = 3$. A tedious algebraic calculation results in the amplitude equations given in Appendix 2. Equations (21) and (29) along with the kinematic condition in (17) constitute what we have already referred to in the Introduction as the TK1[m] model. This model satisfies all temperature boundary conditions at any level of truncation. A summary of all models and associated equations in given in Table 1.

6. Solitary waves

We now seek traveling-wave solutions propagating at a constant speed c. We introduce the moving coordinate transformation $Z = X - c\Theta$ in the long-wave evolution equation (10) with $\partial/\partial\Theta = -c\partial/\partial Z$ for the waves to be stationary in the moving frame. The resulting equation is then integrated once and we fix the integration constant by demanding $h \to 1$ as $Z \to \pm\infty$. This gives

$$h''' = \frac{(h-1)[3c - 2(h^2+h+1)]}{2h^3} - \mathcal{A}(h)h' - \mathcal{B}(h)h'^2 - \mathcal{C}(h)h'', \tag{31}$$

where the primes denote differentiation with respect to Z. This equation together with the boundary conditions $h \to 1$ as $Z \to \pm\infty$ and all the derivatives of h approaching zero as $Z \to \pm\infty$ define a nonlinear eigenvalue problem for the solitary wave speed c obtained from LWE.

Similarly, introducing the moving coordinate in the kinematic boundary condition in (17) yields $-ch_Z + q_Z = 0$. This can be integrated once and we fix the integration constant by demanding $h, q \to 1,2/3$ as $Z \to \pm\infty$. This gives a relation between the flow rate and the film thickness

$$q = \frac{2}{3} + c(h-1). \tag{32}$$

We also introduce the moving coordinate transformation in (21) and (26) and after utilizing (32) we obtain

$$\begin{aligned} h''' \;=\; & \frac{(h-1)[3c-2(h^2+h+1)]}{2h^3} + h'\frac{\cot\theta}{\mathrm{We}^{1/3}} + \frac{3\mathrm{Ma}}{2\mathrm{We}^{1/3}h}\tau' + \\ & \frac{3\mathrm{Re}h'}{35\mathrm{We}^{1/3}h^3}\left(c^2h^2 + ch(c-\frac{2}{3}) - (2-3c)^2\right) \end{aligned} \tag{33}$$

and

$$-c\tau' + \frac{27}{20h}\left[\frac{2}{3} + c(h-1)\right]\tau' + \frac{7}{40h}ch'(\tau-1) + \frac{3\mathrm{We}^{1/3}}{\mathrm{Pe}h^2}[\tau(\mathrm{Bi}h+1)-1] = 0. \tag{34}$$

Equations (33) and (34) are subject to the boundary conditions $h(\pm\infty) = 1$ and $\tau(\pm\infty) = 1/(1+\mathrm{Bi})$.

In the moving frame the system of equations in (29) becomes:

$$\frac{\mathrm{Pe}}{\mathrm{We}^{1/3}}\left(\underline{\underline{M_a}}\,\underline{A}_Z + \underline{\underline{M_b}}\,\underline{A} + \underline{d}\right) = \underline{\Delta} + \underline{\underline{M_\Gamma}}\,\underline{A}, \tag{35}$$

where $[\underline{\underline{M_a}}]_{ij} = a_{ij}$ and $[\underline{\underline{M_b}}]_{ij} = b_{ij}$ with $a_{ij} = < w_j, (u^{(0)} - c)\phi_i >$, $b_{ij} = < w_j, (u^{(0)} - c)\phi_{i_Z} + \epsilon\mathrm{We}^{1/3}v^{(0)}\phi_{i_y} >$ and $d_j = < w_j, (u^{(0)} - c)\phi_{0_Z} + \epsilon\mathrm{We}^{1/3}v^{(0)}\phi_{0_y} >$. Note that $\epsilon\mathrm{We}^{1/3}v^{(0)} \equiv -\int_0^y u_Z^{(0)}\mathrm{d}y'$ and so $\epsilon\mathrm{We}^{1/3}v^{(0)}$ has no explicit ϵ and We dependence so that Equation (35) is independent of ϵ (as it should). Equations (33) and (35) are subject to the boundary conditions $h(\pm\infty) = 1$, $\tau(\pm\infty) = 1/(1+\mathrm{Bi})$ and $A^i(\pm\infty) = 0$.

The aim here is to construct the solitary wave solutions of the above models. Such solitary waves correspond to homoclinic orbits of the above dynamical systems. We construct numerically these solutions by using the continuation software AUTO97 [18]. For this purpose the above equations are converted into systems of first-order ordinary differential equations. However, when the Galerkin projection is employed for the temperature field, the system in (35) can have a singular point somewhere in the domain, let us say at $Z = Z_0$. This is due to the fact that with the Galerkin projection the ij element of the matrix $\underline{\underline{M_a}}$ is $\int_0^1 (u^{(0)} - c)\phi_i\phi_j\mathrm{d}\eta$. As the interfacial waves become larger, the flow becomes faster so that the term $u^{(0)} - c$ which is strictly negative for small amplitude waves, passes through zero and becomes positive. Note that in the absence of Marangoni effects $u^{(0)} = c$ on the interface when $h = 3 - (2/c)$. Hence, as the height of the waves increases: the inner product $\int_0^1 (u^{(0)} - c)\phi_i\phi_j\mathrm{d}\eta$ can in fact change sign and become positive (recall that the ϕ_i's are non-negative). We then infer that the determinant of $\underline{\underline{M_a}}$ can pass through zero for sufficiently large waves. This can be easily illustrated for the simple cases $m = 1$ and $m = 2$ while our numerical computations show that this is also the case for $m \geq 3$. This singularity would then cause some formidable difficulties in the numerical solution of (33) and (35) when it comes to matrix inversion.

Despite the fact that (35) has a singular point at $Z = Z_0$ one can still compute a Taylor series expansion of $\underline{A}$ from (35) anywhere in the domain: simply substitute in (35) the Taylor series for $\underline{A}$ about $Z = Z_0$ and obtain a sequence of equations for the coefficients of the expansion. This formal expansion procedure does not break down and hence $\underline{A}$ is analytic throughout the domain. Following also the classification given by Bender and Orszag [19] the singular point is an 'irregular singular point'; in general, for such points some of the solutions may not have an essential singularity and may even be analytic at these points.

One could then develop a more sophisticated numerical scheme to utilize a truncated series expansion at $Z = Z_0$ obtained analytically and evaluate the derivatives away from the singularity. That would also require matching of the local analytical solution to the numerical solution away from the singularity. However, we can bypass this more involved procedure by appropriately modifying our projection approach. More specifically, we introduce the weight functions

$$w_j = (u^{(0)} - c)\phi_j \tag{36}$$

so that the *ij* element of the coefficient of $\underline{A}_Z$ in Equation (35), $\underline{\underline{M_a}}$, now becomes $\int_0^1 (u^{(0)} - c)^2 \phi_i \phi_j \mathrm{d}\eta$. For $m = 1$ the determinant of $\underline{\underline{M_a}}$ is just $\int_0^1 (u^{(0)} - c)^2 \phi_1^2 \mathrm{d}\eta > 0$ while for $m = 2$ it is $(\int_0^1 (u^{(0)} - c)^2 \phi_1^2 \mathrm{d}\eta)(\int_0^1 (u^{(0)} - c)^2 \phi_2^2 \mathrm{d}\eta) - (\int_0^1 (u^{(0)} - c)^2 \phi_1 \phi_2 \mathrm{d}\eta)^2 > 0$ from Schwarz's inequality. In fact, our computations indicate that the determinant remains positive for all m. Hence, the weight functions in (36) are introduced for numerical convenience only, as they convert (35) to a system without any singular points. This new system and (33) constitutes what we have already referred to in the Introduction as the TK2[m] model.

An analysis similar to that in Section 5.1 now indicates that for $m \geq 3$ the system of equations obtained with the modified projectjon method yields, with an appropriate expansion, the long-wave theory in the moving frame. This is not surprising as we also needed $m \geq 3$ to obtain the long-wave theory from the time-dependent system in (29). Although 3 is the minimum dimensionality for the modified system using the weights in (36) to fully resolve the behavior of small amplitude waves, for convenience we shall investigate the model obtained at the lower possible level of truncation, *i.e.* for $m = 1$. This yields the following equation for the interfacial temperature

$$\begin{aligned}
0 \;=\; & \mathrm{Pe}\tau'(3c-2)^2\left(\frac{5287}{144}+\frac{45}{4}\mathrm{Bi}h+\frac{161}{144}\mathrm{Bi}^2h^2\right)\\
& +\mathrm{Pe}\tau' c^2h^2\left(\frac{665}{24}+\frac{175}{24}\mathrm{Bi}h+\frac{2}{3}\mathrm{Bi}^2h^2\right)\\
& -\mathrm{Pe}(3c-2)ch\tau'\left(\frac{8215}{144}+\frac{1021}{72}\mathrm{Bi}h+\frac{163}{144}\mathrm{Bi}^2h^2\right)\\
& +\mathrm{PeBi}\tau h'\left((3c-2)^2\left(\frac{45}{8}+\frac{161}{144}\mathrm{Bi}h\right)+\mathrm{Bi}ch^2\left(\frac{11}{64}ch-\frac{41}{36}(3c-2)\right)\right)\\
& +\mathrm{Pe}ch'(\tau-1)\left(\frac{301}{192}ch-\frac{61}{6}(3c-2)\right)\\
& +\mathrm{Pe}chh'\left(-\frac{4928\tau-1467}{576}(3c-2)+\frac{101\tau-2}{96}\mathrm{Bi}ch\right)\\
& +\frac{11}{8h}(\tau(1+\mathrm{Bi}h)-1)((2-3c)(149+23\mathrm{Bi}h)+(111+13\mathrm{Bi}h)ch).
\end{aligned} \tag{37}$$

Table 2. Summary of equations for the different traveling wave models. m is the number of modes for the temperature field.

LWE	Improved KKD	TK1[m]	TK2[1]	2D energy model
(31)	(33)	(33)	(33)	(33)
	(34)	(35) with $w_i = \phi_i$	(37)	(41)

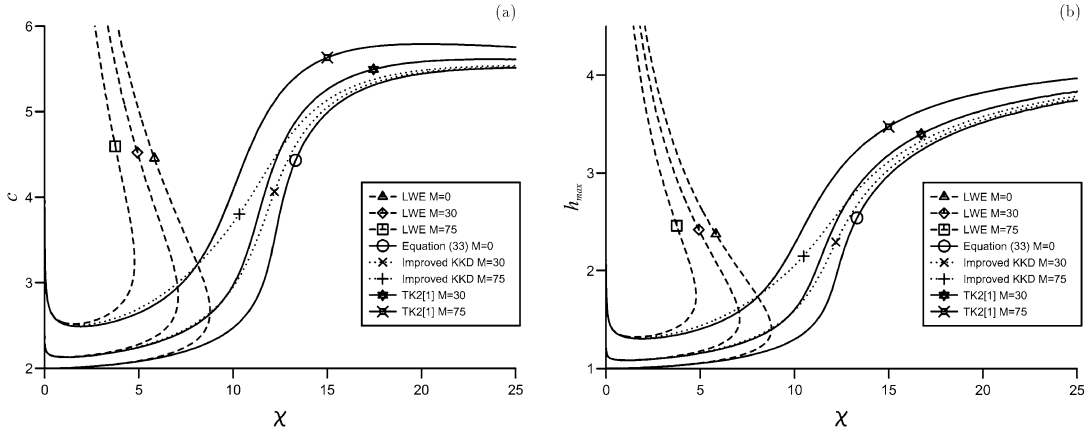

Figure 2. Bifurcation diagrams for the stationary solitary pulses obtained from different models for Pr = 1 and different values of M. In all our computations we take $\theta = \pi/2$, Ka = 3000 and $B = 0{\cdot}1$; (a) speed c as a function of the modified Reynolds number χ; (b) maximum amplitude $h_{\max}$ as a function of modified Reynolds number χ.

The TK2[3] system of the 3 amplitude equations obtained using the modified weights in (36) is a lot more complex than the system of the 3 amplitude equations in the moving frame obtained from the Galerkin projection TK1[3]. Hence, the relative simplicity of the one-mode approximation in (37) makes it an attractive prototype for numerical scrutiny.

We now contrast the solitary pulse solutions obtained from the LWE model in (31), the improved KKD model in (33,34) and the one-mode TK2[1] model in (33,37). A summary of all traveling-wave models is given in Table 2. In all our computations we take $\theta = \pi/2$. Figures 2 and 3 depict the solitary wave speed c and maximum amplitude $h_{\max}$ as a function of the modified Reynolds number χ for Pr = 1 and Pr = 7, respectively and different values of the modified Marangoni number, M. Note that for $M = 0$ both the improved KKD and TK2[1] models give the same bifurcation diagrams as in this limit the energy equations in (34) and (37) are decoupled from the momentum equation in (33).

These bifurcation diagrams are in qualitative agreement with those obtained by Kalliadasis *et al.* [9] for the Joo *et al.* [8] long-wave equation and the KKD model. We first discuss the branches obtained from the improved *KKD* and TK2[1] models. As $\chi \to 0$ both speed and maximum amplitude of the solitary pulses tends to infinity for $M > 0$. This unusual behavior was first pointed out by Kalliadasis *et al.* [9]. The same authors also emphasized that this blow up is not a true singularity formation as other forces which would arrest the singularity are present in the limit $\chi \to 0$. These are the long-range attractive van der Waals interactions between the solid and the gas phase separated by the liquid phase. We note here that if the film thickness tends to zero, the viscous dissipation u_{yy} tends to infinity. The only way to balance an infinite dissipation is via a curvature discontinuity (infinite h_{xxx} – see *e.g.* Equation

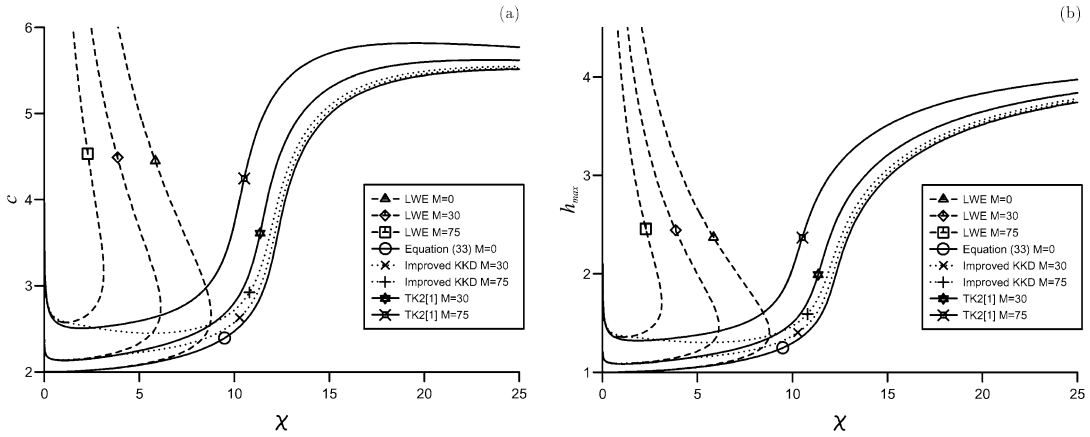

Figure 3. Bifurcation diagrams for the stationary solitary pulses obtained from different models for Pr = 7 and different values of M; (a) speed c as a function of χ; (b) maximum amplitude $h_{\max}$ as a function of χ.

(13)). Hence, in this region of small film thicknesses, the interface develops cusps, unless of course van der Waals interactions with a negative Hamaker's constant are included, *i.e.*, for a completely wetting fluid.

It is also important to point out that the limit $\chi \to 0$ can be achieved either with small film thickness or large viscosity. In the latter case there would be no singularity formation for small χ, instead all curves would start from the infinitesimal wave speed $c = 2$ as the $M = 0$ curve does. Now a parameterization different to the one adopted at the end of Section 2 would be required. In this case one can show from a weakly nonlinear analysis of the LWE model in (9) that dispersion (associated here with the convective-heat-transport term in (9)) can become large close to criticality leading to a Kawahara equation with large dispersion and with solutions which approach Korteweg-de Vries solitons in this limit [20]. Here we assume that χ changes through variation of the film thickness.

For sufficiently large χ the speed and maximum amplitude of our solitary pulses asymptote towards limit values. In fact, as was pointed out by Kalliadasis *et al.* [9], we expect that the different M curves should merge into a single curve (the one obtained from Equation (33) for $M = 0$) in the region of large χ and hence large film thicknesses as in this region the interfacial Marangoni effects are not important compared to the dominant inertia forces and the influence of the temperature field on the hydrodynamics is small. Here we do not track the solution branches beyond $\chi = 25$. Besides, in this region of relatively large χ the capillary forces are probably not strong enough to stabilize the large destabilizing inertia effects and 1D solitary pulses might develop instabilities in the transverse direction. Note that in all cases, fixing Pr and increasing M increases c and $h_{\max}$. On the other hand fixing M and increasing Pr decreases c and $h_{\max}$ for moderate χ while c and $h_{\max}$ slightly increase as Pr increases in the regions of small and larger χ.

We now examine the LWE model. Unlike the bifurcation diagrams for the improved KKD and TK2[1] models which predict the continuing existence of solitary pulses for all χ, LWE exhibits limit points and branch multiplicity with two branches, a lower branch and an upper branch. These limit points occur at specific values of χ which depend on both M and Pr. For the isothermal falling film problem, Pumir *et al.* [21] demonstrated that the long-wave expansion exhibits a finite-time blow-up behavior for sufficiently large sets of smooth initial data when this equation is integrated in time for Reynolds numbers larger than those corres-

ponding to the turning points. Obviously this unrealistic behavior is related to the model's non-existence of solitary waves. A similar catastrophic behavior is also observed with our LWE model in the presence of Marangoni effects.

7. Small film thicknesses

For small χ the lower branch obtained from LWE also blows up to infinity. This lower branch is in agreement with the improved KKD and TK2[1] models. The agreement persists up to an $O(1)$ Reynolds number which is fairly close to the turning point. A similar agreement was found by Kalliadasis *et al.* [9] for the KKD and Joo *et al.* [8] models. Kalliadasis *et al.* demonstrated by performing a small χ expansion that the agreement between the KKD and Joo *et al.* models is due to the fact that in the region of small film thicknesses, where the Marangoni forces dominate over inertia forces, the two models reduce to the same equation for the film thickness and hence in this limit both approximations are identical.

Here we demonstrate that all models, KKD, Joo *et al.*, LWE, improved KKD and TK1[m] are identical in this limit. From $\mathrm{Pe} = \mathrm{PrRe} = (\chi \sin\theta)/2$, $\mathrm{Pe} \to 0$ as $\chi \to 0$. Hence, to leading order, the convective terms in the heat transport equation can be neglected slaving the interfacial temperature to the free-surface height in the form

$$\tau = \frac{1}{1 + \mathrm{Bi}h} \sim 1 - B\chi^{1/3}h + O(\chi^{2/3}). \tag{38}$$

Similarly, to leading order, the inertia term can be neglected from the momentum equations in (20) and (21). It is now obvious why the different approximations lead to the same equation as $\chi \to 0$: all models for the interfacial temperature yield the expression in (38) while in the absence of inertia all momentum equations are identical (recall that (21) corrects the critical Reynolds number obtained from (20)). Substituting now (38) in the momentum equation gives

$$q \sim \frac{2h^3}{3} + \frac{2\mathrm{Ka}h^3}{3\sin\theta}\chi^{-2/3}h_{xxx} + \frac{MB}{\sin\theta}\chi^{-1/3}h^2h_x, \tag{39}$$

which is also identical to the LWE flow rate. This also implies that it is the inertia term (8/15) $\mathrm{Re}\, h^6h_x$ which is responsible for the upper branch of LWE (even though this term yields the exact critical condition).

Substituting now (39) in the kinematic boundary condition (17) yields the evolution equation

$$h_t + 2h^2h_x + \left(\frac{2\mathrm{Ka}h^3}{3\sin\theta}\chi^{-2/3}h_{xxx} + \frac{MB}{\sin\theta}\chi^{-1/3}h^2h_x\right)_x \sim 0,$$

which after rescaling space with $\chi^{-1/6}\sqrt{\frac{2\mathrm{Ka}}{3MB}}$ and time with $(3/2)\chi^{-1/6}\sqrt{\frac{2\mathrm{Ka}}{3MB}}$ gives the evolution equation

$$h_t + \left(h^3 + \frac{h^3}{\delta}h_{xxx} + \frac{h^2}{\delta}h_x\right)_x \sim 0, \tag{40a}$$

which contains a single parameter

$$\delta = \chi^{1/6}\sin\theta\sqrt{\frac{2^3\mathrm{Ka}}{3^3M^3B^3}}. \tag{40b}$$

Hence, in the limit of $\chi \to 0$, *all* models reduce to the single evolution equation in (40a) and the behavior of the film depends on δ only and it is *universal* for all values of the governing dimensionless groups. Note that the χ-expansion performed here should not be confused with the ϵ-gradient expansion for fixed χ performed for the TK1[m] model to fully recover the LWE model.

We should point out that the transformation to obtain (40a) shows that the nonlinear convective term $(h^3)_x$ and the two surface-tension forces balance as $\chi \to 0$. In this limit, both capillary and Marangoni forces scale as $1/\delta$ with $\delta \to 0$. For a falling film in the absence of Marangoni effects, the destabilising inertia terms are vanishing in the limit $\chi \to 0$ while in our case, the destabilising terms are interfacial forces and are still present as $\chi \to 0$. The stabilising terms are also interfacial forces with exactly the same dependence on δ.

Figure 4 shows typical solitary wave shapes for both free surface and interfacial temperature in the region of small χ obtained from the three models for $M = 75$. Note that only part of the actual computational domain, which is [0, 150], is shown here. As expected, the solitary pulses obtained from all three models are indistinguishable in this region. For example changing Pr from 1 to 7 does not influence the pulses. The shape of the free-surface solitary waves is qualitatively similar to the solitary pulses computed for the isothermal film and it consists of a primary solitary hump with a gentle sloping back edge and a steep front edge preceded by a series of small, decaying bow waves.

8. Finite-differences solution for the energy equation

In Figure 5 we compare, for the particular case $M = 0$, the interfacial temperature distributions obtained from the improved KKD and TK2[1] models with the solution of the energy equation in (24)

$$T_{\eta\eta} = \frac{\mathrm{Pe}}{\mathrm{We}^{1/3}} \left(\left(\frac{3}{2} q h (2\eta - \eta^2) - c h^2 \right) T_Z + \frac{c}{2} h h_Z \eta(\eta - 1)(\eta - 2) T_\eta \right) \tag{41a}$$

subject to the boundary conditions for the temperature in (5e) and (22)

$$T = 1 \quad on \quad \eta = 0, \quad T_\eta = -\mathrm{Bi} h T \quad on \quad \eta = 1 \tag{41b}$$

solved in 2D along with periodic boundary conditions in the z-direction and where q is given in Equation (32). We shall refer to the system in (33) and (41) as the '2D energy model'. The energy equation was solved numerically using an implicit finite-differencing scheme. For $M = 0$, the energy equation is decoupled from the momentum equation in (33) which is then used to obtain the free surface and corresponding flow field.

Clearly, for the moderate value $\chi = 5$, the improved KKD, TK2[1] and 2D energy model give quite similar interfacial-temperature distributions with the TK2[1] model being graphically indistinguishable to the finite differences solution. The agreement persists for the larger value $\chi = 10$ and $\mathrm{Pr} = 1$. However for $\chi = 10$ and $\mathrm{Pr} = 7$ we notice a difference between the improved KKD model and the 2D energy model and TK2[1] model. The difference increases further as we increase the Reynolds number up to $\chi = 15$. In this region of 'large' Reynolds numbers, for $\mathrm{Pr} = 1$, the TK2[1] model is in very good agreement with the 2D energy model solution while for $\mathrm{Pr} = 7$ a small difference between the two is observed. This is quite encouraging and implies that the TK2[1] model provides a good representation of the interfacial temperature field even for 'large' Reynolds and Péclet numbers at least in the region of small Marangoni numbers.

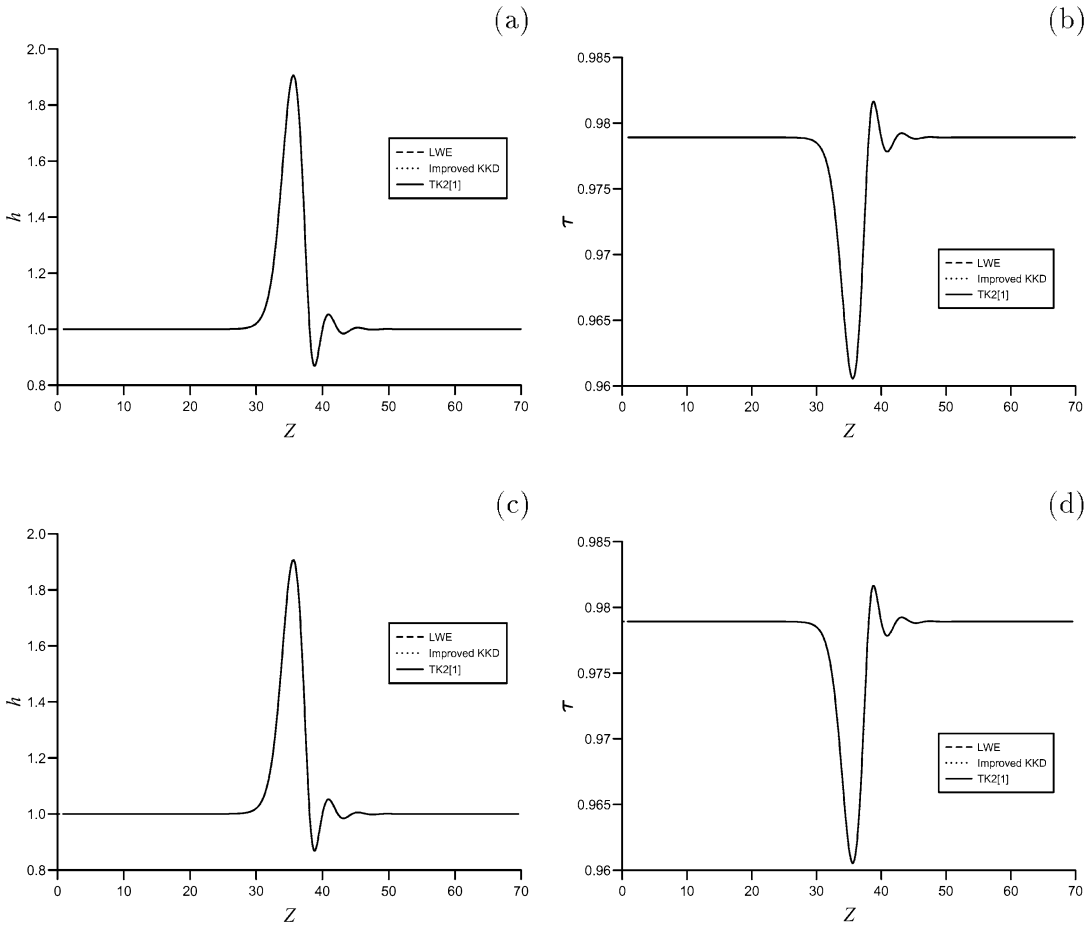

Figure 4. Solitary pulses for the free surface and interfacial temperature with $\chi = 0{\cdot}01$ and $M = 75$. $\mathrm{Pr} = 1$ in (a) and (b) and $\mathrm{Pr} = 7$ in (c) and (d).

One way to compute the temperature field for $M \neq 0$ would be to set up an iterative scheme coupled with a domain perturbation approach, however, this was not done here. It is important to emphasize that even the simple equation in (41) is computationally much more demanding than Equations (34) and (37). Hence, from both the computational and analytical point of view, dealing with sets of partial differential equations for interfacial quantities and of reduced spatial dimension (1 in (34) and (37) instead of 2 in (41)) is much more attractive. At the same time the models in (34) and (37) retain the most relevant physical features of the problem and hence they can contribute to the understanding of the dynamics of the film without resorting to a numerical study of the full Navier-Stokes/energy equations.

Figure 6 depicts typical solitary waves obtained from all three models for the moderate value $\chi = 5$ and two different Prandtl numbers, $\mathrm{Pr} = 1$ and $\mathrm{Pr} = 7$, for $M = 30$. For the 'small' value $\mathrm{Pr} = 1$ all three approaches give similar results for both free surface and interfacial temperature. However, by increasing the Prandtl number to the 'large' value $\mathrm{Pr} = 7$, we notice a significant difference between LWE and the other two models which give similar solitary pulses. This difference is due to the fact that increasing the Prandtl number increases the vertical heat flux. This flux is not represented properly by LWE despite the fact that it has

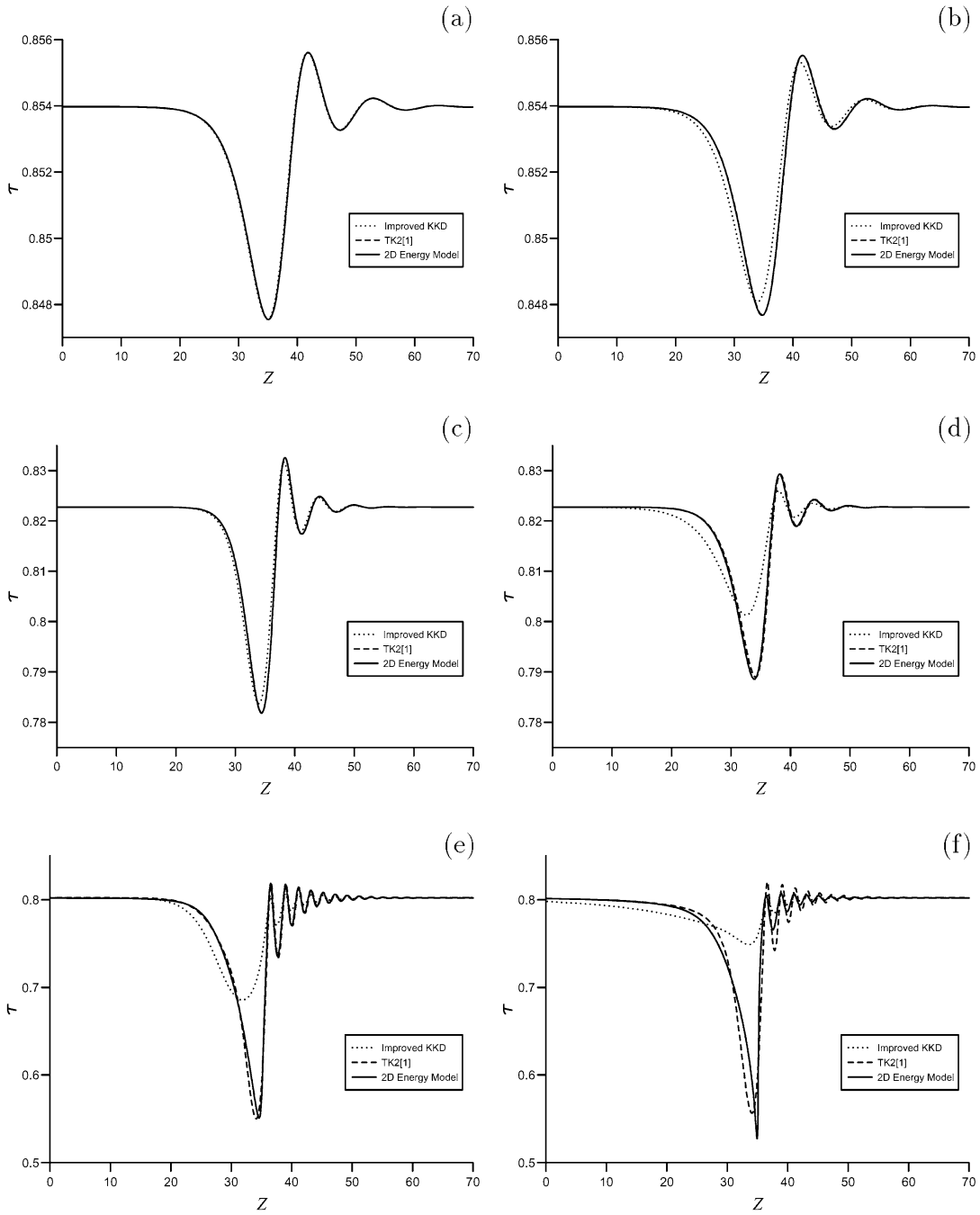

Figure 5. Comparison of the interfacial temperature distribution obtained from the improved KKD and TK2[1] models with that obtained from the energy equation in (41) for $M = 0$; (a) $\mathrm{Pr} = 1$, $\chi = 5$; (b) $\mathrm{Pr} = 7$, $\chi = 5$; (c) $\mathrm{Pr} = 1$, $\chi = 10$; (d) $\mathrm{Pr} = 7$, $\chi = 10$; (e) $\mathrm{Pr} = 1$, $\chi = 15$; (f) $\mathrm{Pr} = 7$, $\chi = 15$.

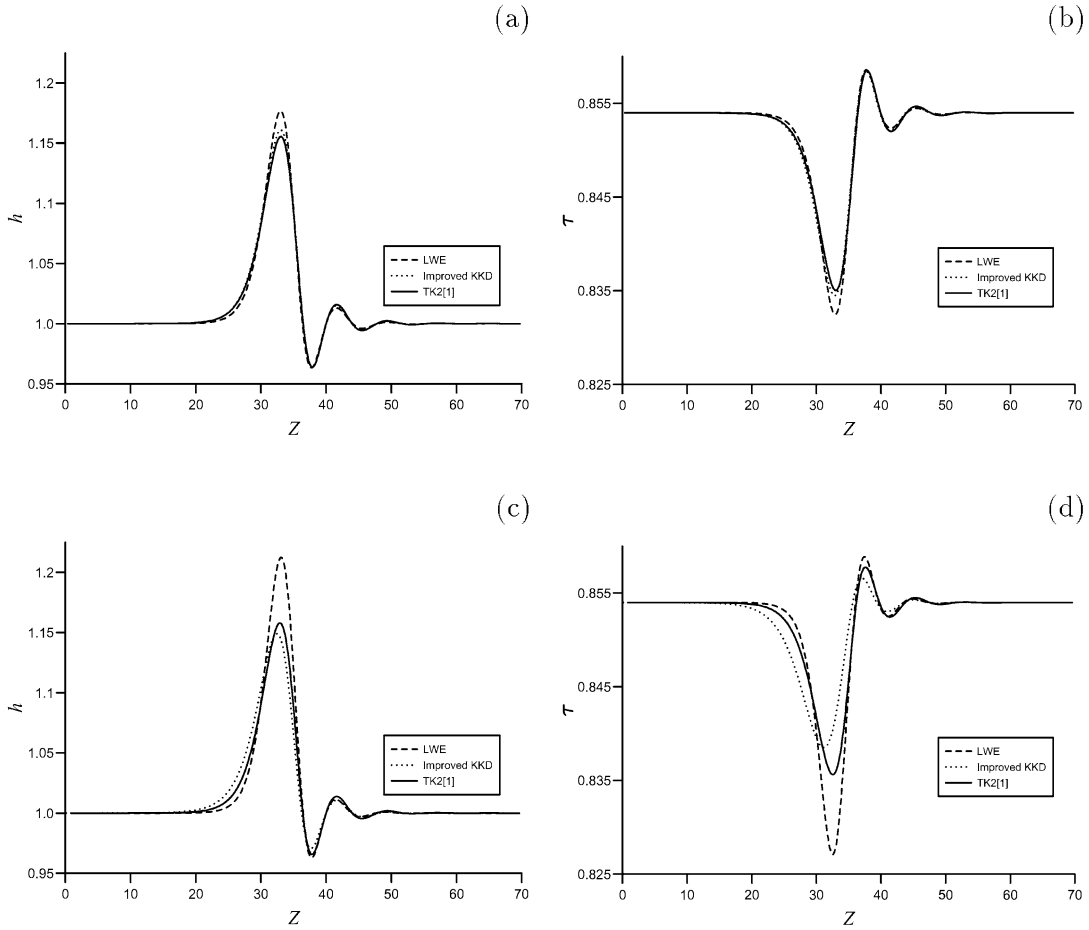

Figure 6. Free surface and interfacial temperature obtained from LWE, improved KKD and TK2[1] models for $\chi = 5$ and $M = 30$. Pr = 1 in (a) and (b) and Pr = 7 in (c) and (d).

been derived based on a large Peclet number assumption in order to include the convective heat transport effects at a low relevant order.

Figure 7 shows typical solitary pulses for the 'large' value $\chi = 15$, $M = 75$ and two different Prandtl numbers, Pr = 1 and Pr = 7. We observe a divergence between the models as Pr increases. The interfacial temperature of the improved KKD model is dampened when Pr increases while the TK2[1] model gives a much larger variation for the interfacial temperature with the peak of the wave being cooler than that predicted by the improved KKD model. A comparison with Figures 4–6 shows that increasing χ increases the amplitude of the bow waves in front of the primary hump for both free surface and interfacial temperature pulses. This is simply due to the fact that increasing χ increases energy dissipation.

Figure 8 depicts the streamlines and isotherms at $\chi = 13$, Pr = 7 and two different values of M, $M = 0$ (Figures 8(a–d) and $M = 30$ (Figures 8(e,f)). For $M = 0$, the isotherms obtained from the TK2[1] model are close to the isotherms obtained from the 2D energy model while a significant difference between the improved KKD and 2D energy models is observed. The minimum of the temperature obtained from the TK2[1] model ($\sim$0·65) is in excellent agreement with the minimum obtained from the 2D energy model ($\sim$0·66). This

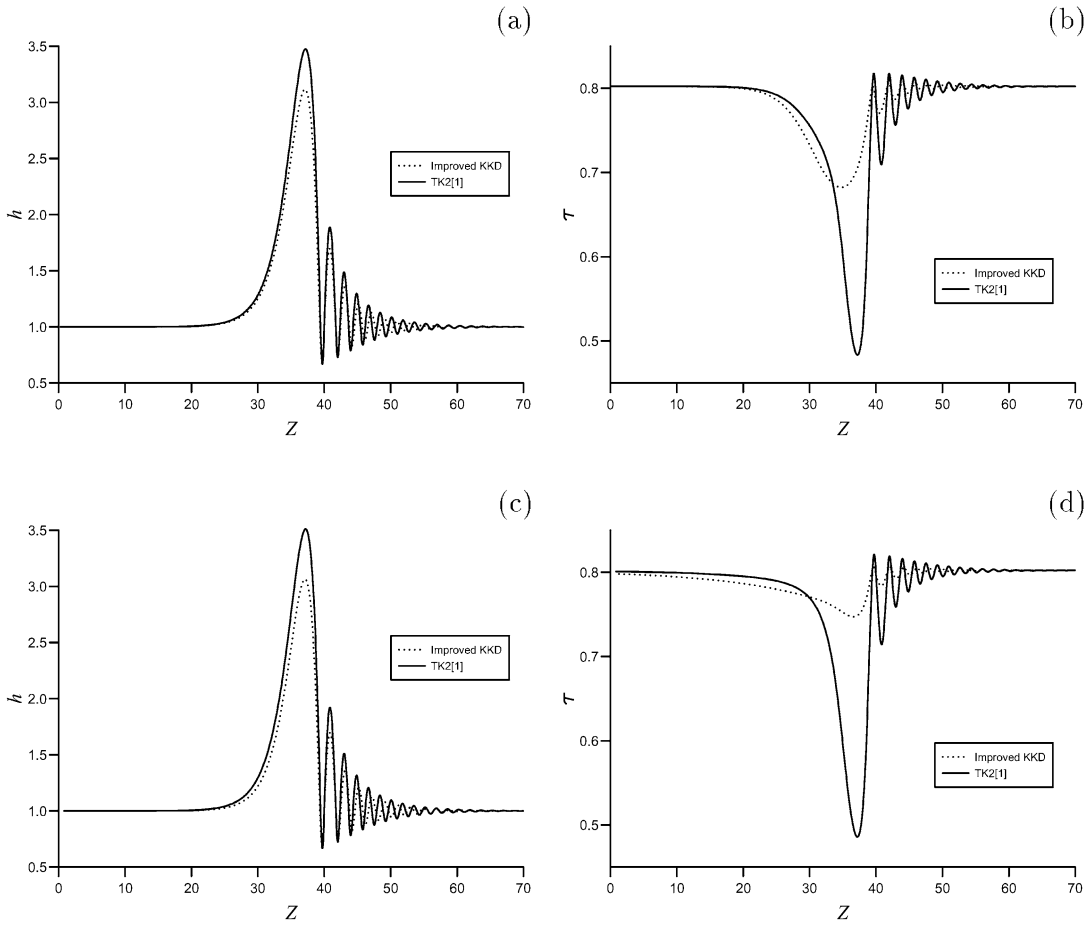

Figure 7. Free surface and interfacial temperature obtained from the improved KKD and TK2[1] models for $\chi = 15$ and $M = 75$. Pr = 1 in (a) and (b) and Pr = 7 in (c) and (d).

minimum always appears close to the peak of the wave as this is the area further away from the wall and hence the coldest area in the wave. The improved KKD model predicts a hotter peak with a temperature $\sim 0{\cdot}77$. Note also that a similar computation for smaller Pr and χ values shows that the isotherms are nearly aligned with the wall as expected since for small Péclet numbers the temperature field is nearly a linear function of y. For the 'large' values of χ and *Pr* used here, the isotherms are not aligned with the wall and are deflected upwards due to the motion of the fluid under the wave crest.

For $M = 30$, Figures 8(e,f) show that the Marangoni effect now enhances the speed and amplitude of the solitary waves. As a consequence, for the particular values chosen here, a clockwise recirculation zone forms under the wave crest. The fluid is effectively pushed by the thermo capillary Marangoni stresses from the back of the wave to the front. Now the solitary waves transport mass as the fluid in the solitary hump is trapped. Such recirculation zones are of paramount significance in mass transport applications.

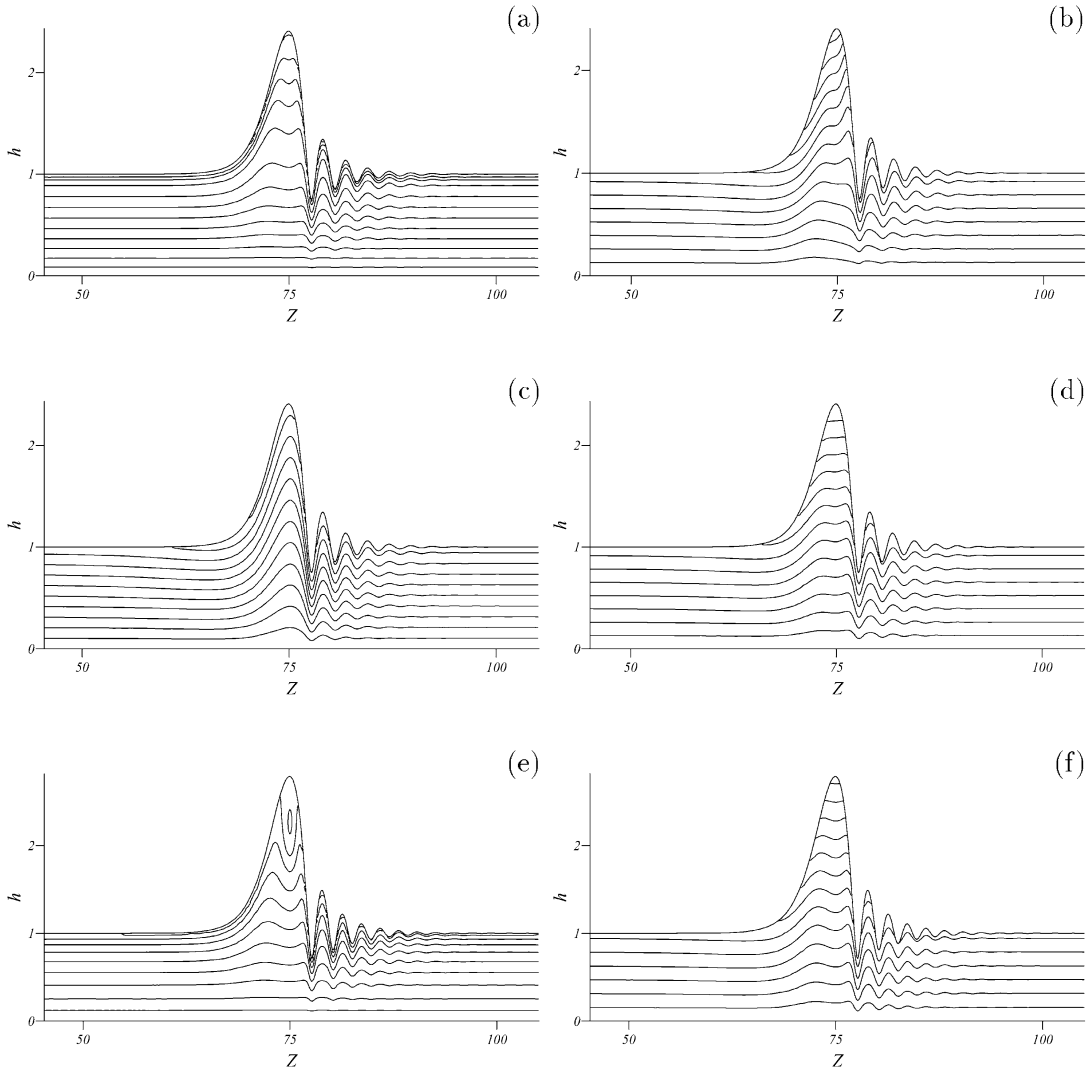

Figure 8. Streamlines and isotherms for $\chi = 13$ and $\mathrm{Pr} = 7$. (a) and (e) show streamlines obtained from the TK2[1] model for $M = 0$ and $M = 30$, respectively. The corresponding wave velocities are $c = 4{\cdot}24$ and $c = 4{\cdot}81$. (d) and (f) show the isotherms from the TK2[1] model for $M = 0$ and $M = 30$, respectively. (b) and (c) are isotherms at $M = 0$ of the 2D energy model and the improved KKD model, respectively. The isotherms in (b) and (d) are uniformly separated by temperature intervals of 0·025, from 1 to 0·675. The isotherms in (c) are uniformly separated by temperature intervals of 0·02, from 1 to 0·78. Finally, the isotherms in (f) are uniformly separated by intervals of 0·03, from 1 to 0·61.

9. Evolution toward solitary waves

The simplicity of the time-dependent improved KKD model in Equations (17), (21) and (26) allows us to address one important issue: what is the spatial-temporal evolution of our system. In addition, for the parameter values chosen here the stationary solitary wave solutions of the improved KKD model are close to those obtained from the TK2[1] model suggesting a similar time-dependent behavior.

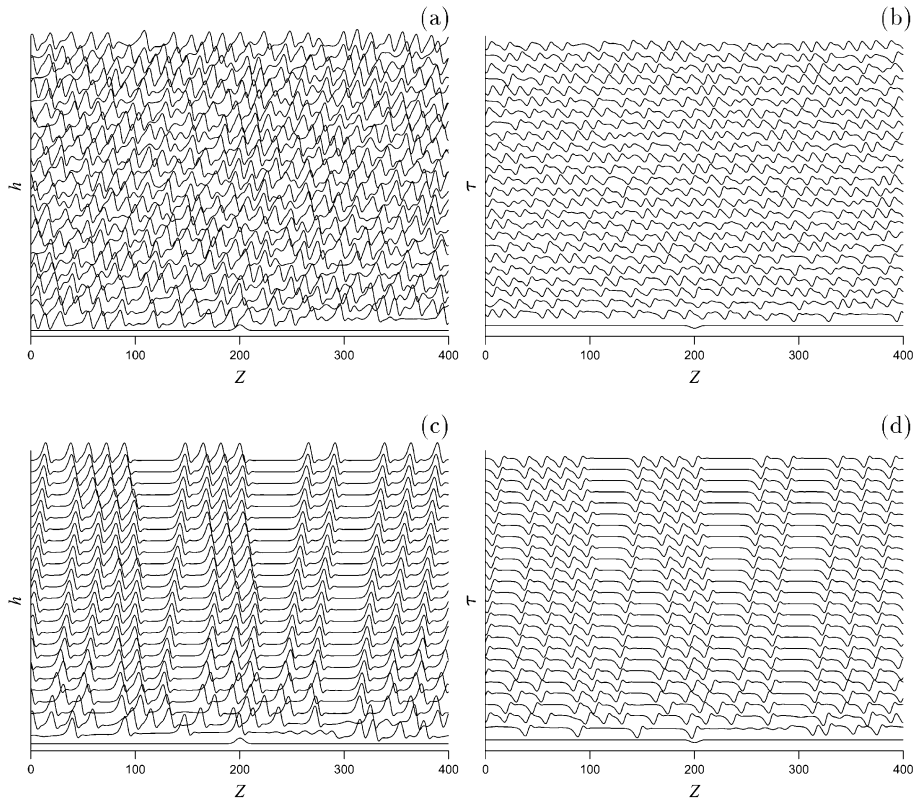

Figure 9. Time evolution for the free surface in (a,c) and interfacial temperature in (b,d) in an extended domain obtained from the improved KKD model for $X = 5$ and $M = 30$. Pr $= 1$ in (a,b) and the coordinate system is moving with velocity 2. Pr $= 7$ in (c,d) and the coordinate system is moving with velocity 2·084. Successive curves are separated by $\Delta\Theta = 10^3$ with $\Theta \in [0{,}2{\cdot}5 \times 10^4]$.

For our computations we employed a Crank-Nicolson-type implicit scheme with the spatial derivatives approximated by central differences and with dynamic time step adjustment. We impose periodic boundary conditions over a finite domain much larger than the maximum growing wavelength predicted by linear stability. The computations are performed in the moving frame $Z = (x - 2t)/(\epsilon \mathrm{We}^{1/3})$.

Some typical time evolutions are shown in Figures 9 and 10. Within the inception region the wave amplitude grows exponentially in time, as predicted by linear stability. Immediately beyond it, the waves begin to steepen in front and develop a back shoulder, signifying a weakly nonlinear excitation of an overtone. The amplitude modulation still persists, however, the larger waves now begin to accelerate, they collide with the smaller waves in front of them and eventually overtake them. This coalescence process is evident for both free surface and interfacial temperature. The final result of the evolution is a train of soliton-like coherent structures with almost the same amplitude and which interact indefinitely with each other like in soliton-soliton elastic collision. These coherent structures possess a gently sloping back egde and a steep front edge preceded by some small bow waves and are reminiscent of the solitary-wave coherent structures observed in the bifurcation diagrams of Figures 2, 3 for the stationary solitary wave solutions for free surface and interfacial temperature.

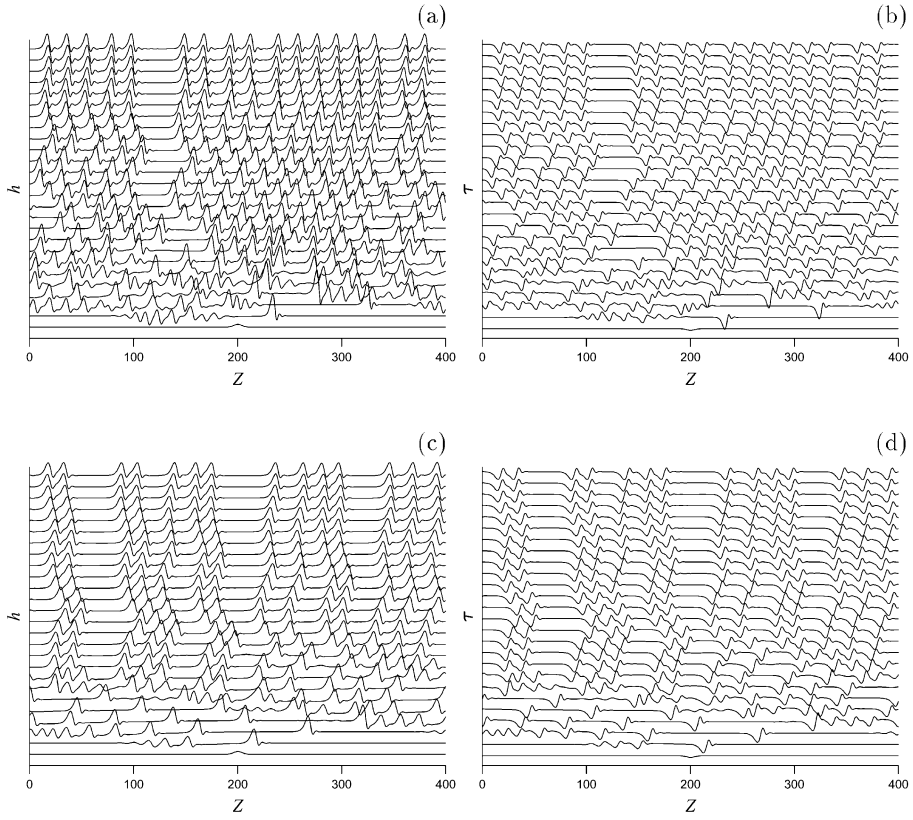

Figure 10. Time evolution for the free surface in (a,c) and interfacial temperature in (b,d) in an extended domain obtained from the improved KKD model for $\chi = 10$ and $M = 30$. Pr $= 1$ in (a, b) and the coordinate system is moving with velocity 2·176. Pr $= 7$ in (c,d) and the coordinate system is moving with velocity 2·127. Successive curves are separated by $\Delta\Theta = 2 \times 10^2$ with $\Theta \in [0, 5 \times 10^3]$. Note that the actual vertical scale is approximately twice as big as that in Figure 9 so that the amplitudes of the waves in Figure 10 are actually bigger than those in Figure 9.

We have also performed computations for a wider range of the relevant dimensionless groups. These numerical experiments show that increasing χ for fixed Pr increases the average amplitude for both free-surface and interfacial temperature waves. On the other hand, increasing Pr sufficiently for fixed χ organizes the system from a train of strongly interacting solitary waves to a train of weakly interacting solitary waves. Further increases of Pr increase the characteristic wavelength of the solitary waves leading to solitary wave trains separated by relatively flat regions. These observations are illustrated in Figures 9 and 10.

Finally, we should point out that unlike LWE which can exhibit finite-time blow up behavior, our models are quite robust and they do not exhibit any singularity formation. This is illustrated in Figure 10 with values of $\chi = 10$, and $M = 30$ for which Figures 2 and 3 show that LWE does not have any solitary-wave solutions.

10. Conclusion

We have analyzed the dynamics of a thin liquid film falling down a uniformly heated wall. The heat provided by the wall sets up surface tension gradients which induce thermocapillary

Marangoni effects which in turn cause a Marangoni instability which interacts with the usual hydrodynamic mode of instability for an isothermal film.

We revisited the KKD model developed for this flow by Kalliadasis *et al.* [10] and we showed that a simple Galerkin projection for the velocity field with just one test function (a self-similar parabolic profile) and a weight function, taken to be the test function itself, fully corrects the critical Reynolds number obtained from the KKD model. The corrected momentum equation along with the linear self-similar temperature distribution suggested by Kalliadasis *et al.* [10] constitute the 'improved KKD model'. In addition, a long-wave expansion of the equations of motion and free-surface boundary conditions for large Péclet numbers leads to the model equation we referred to as the 'LWE model'.

However, the linear temperature distribution in the improved KKD model does not satisfy all boundary conditions and hence it is not expected to be a very accurate representation of the temperature profile. We then developed a more refined formulation based on a high-order Galerkin projection in terms of polynomial test functions. The temperature distribution is such that it now satisfies all boundary conditions. The resulting amplitude equations for the temperature along with the corrected momentum equation constitute the 'TK1[m] model'. We showed that not only does this model correct the deficiencies of the KKD model, namely predicting the critical Reynolds number with a 20% error, but it also gives the LWE model with an appropriate gradient expansion close to criticality and hence it can accurately describe the dynamics of the film in this region. For this purpose we need at least three amplitude equations for the temperature field. We then truncated the TK1[m] model at $m = 3$ and we offerred a reduced three-amplitude equations model which fully resolves the dynamics close to criticality.

We subsequently focused on the nonlinear stage of the instability with particular emphasis on single-hump solitary waves. We showed that the numerical analysis for the solitary waves is facilitated if the weight functions for the energy equation were appropriately modified. This model was referred to as the 'TK2[m] model'. We contrasted the solitary pulse solutions obtained from the LWE model with those obtained from the improved KKD and TK2[1] models (for simplicity we restricted ourselves to $m = 1$ for the TK2[m] model). We demonstrated that in all cases the solitary wave solution branch obtained from LWE is unrealistic with limit points and branch multiplicity with two branches, a lower branch and an upper branch.

This behavior is similar to what has been observed with isothermal films, where the turning points and non-existence of solitary pulse solutions of the long-wave expansion have been associated with a finite-time blow up behavior, when this equation is integrated numerically in the region where solitary waves do not exist.

The improved KKD and TK2[1] models on the other hand predict the continuing existence of solitary waves for all values of the Reynolds number. These models are then expected to be robust in time-dependent computations. Such computations with the improved KKD model show that for large times the free surface and interfacial temperature approach a train of coherent structures which resemble the infinite-domain stationary solitary pulses obtained in our bifurcation diagrams.

Finally, there are a number of interesting questions related to the analysis presented here. For example, it would be interesting to undertake a detailed numerical study in the region of small χ and in the presence of intermolecular forces. It would also be interesting to extend the present analysis to other situations and related problems where Marangoni effects are present, *e.g.* thin films in the presence of surface active agents (surfactants) that alter the surface tension (solutal Marangoni effect). Another interesting problem is the dynamics of a thin film in the

presence of an exothermic chemical reaction taking place in the film. In this case the heat released by the reaction sets up surface-tension gradients that induce thermocapillary stresses on the free surface, thus affecting the evolution of the film. Trevelyan *et al.* analyzed this problem with a long-wave expansion of the equations of motion and associated wall/free-surface boundary conditions [22]. This is a system with a full feedback mechanism. We are currently investigating the dynamics of a falling film in the presence of chemical reactions by using a high-order Galerkin projection similar to the one employed here [23, 24]. A related system would be a thin film in the presence of surfactants depleted/produced by a chemical reaction. Now the (isothermal) chemical reaction changes the surfactant concentration and this alters the rate by which the surface tension changes as a function of surfactant concentration which in turn affects the interface which then changes the rate of reaction (feedback).

The analysis itself can be refined further by including the second-order dissipative effects associated with both the momentum and energy equations neglected here. Such effects have been shown to modify the amplitude of the front-running capillary waves in isothermal films [14]. This second-order model would require a more detailed description of the velocity field which would not be limited to remain parabolic as in this study. We shall examine this and related problems in a future paper.

Acknowledgements

We are grateful to Christian Ruyer-Quil, Benoit Scheid and Manuel Velarde for numerous stimulating discussions on Marangoni effects in thin films. We acknowledge financial support from the Engineering and Physical Sciences Research Council of England through grant no. GR/S01023 and an Advanced Research Fellowship, grant no. GR/S49520.

Appendix 1: Derivation of the long-wave evolution equation

The LWE is obtained by expanding Equations (4) and (5) for $\epsilon \ll 1$. More specifically, we expand our variables in the forms $u \sim u_0 + \epsilon u_1 + \epsilon^{(2-n)} u_2$, $v \sim v_0 + \epsilon v_1 + \epsilon^{(2-n)} v_2$ and $p \sim p_0 + \epsilon^{(1-n)} p_1$ and $T \sim T_0 + \epsilon^{(1-n)} T_1$. We note that the continuity equation in (4a), $u_x + v_y = 0$ and the no-slip boundary condition in (5e), $v = 0$ on $y = 0$, can be used to obtain v_0, v_1 and v_2 from u_0, u_1 and u_2, respectively. In what follows we assume that Bi, Re, Ma, ϵ^n Pe and ϵ^2 We are all O(1). The leading order terms of the relevant equations then are given by:

$$
\begin{aligned}
&(4b)_0: \ u_{0_{yy}} = -2 \\
&(5e)_0: \ u_0 = 0 \quad \text{on} \quad y = 0 \\
&(5b)_0: \ u_{0_y} = u_0 \quad \text{on} \quad y = h
\end{aligned}
$$

$$
\begin{aligned}
&(4c)_0: \ p_{0_y} + \cot\theta = 0 \\
&(5a)_0: \ p_0 = -\epsilon^2 \mathrm{We} h_{xx} \quad \text{on} \quad y = h
\end{aligned}
$$

$$
\begin{aligned}
&(4d)_0: \ T_{0_{yy}} = 0 \\
&(5e)_0: \ T_0 = 1 \quad \text{on} \quad y = 0 \\
&(5c)_0: \ T_{0_y} = -\mathrm{Bi} T_0 \quad \text{on} \quad y = h
\end{aligned}
$$

These yield

$$
u_0 = 2hy - y^2, \quad p_0 = (h - y)\cot\theta - \epsilon^2 \mathrm{We} h_{xx} \quad \text{and} \quad T_0 = 1 - \frac{\mathrm{Bi} y}{(1 + \mathrm{Bi} h)}.
$$

The $O(\epsilon)$ terms of the equations are given by:

$$(4b)_1: \; u_{1_{yy}} = 2p_{0_x} + \mathrm{Re}(u_{0_t} + u_0 u_{0_x} + v_0 u_{0_y})$$
$$(5e)_1: \; u_1 = 0 \quad \text{on} \quad y = 0$$
$$(5b)_1: \; u_{1_y} = -2\mathrm{Ma}(T_{0_x} + hT_{0_y}) \quad \text{on} \quad y = h$$

and the $O(\epsilon^{1-n})$ terms of the equation are

$$(4c)_{1-n}: \; p_{1_y} = 0$$
$$(5a)_{1-n}: \; p_1 = 0 \quad \text{on} \quad y = h$$

$$(4d)_{1-n}: \; T_{1_{yy}} = \epsilon^n \mathrm{Pe}(T_{0_t} + u_0 T_{0_x} + v_0 T_{0_y}$$
$$(5e)_{1-n}: \; T_1 = 0 \quad \text{on} \quad y = 0$$
$$(5c)_{1-n}: \; T_{1_y} = -\mathrm{Bi} T_1 \quad \text{on} \quad y = h$$

These yield

$$\begin{aligned} u_1 \; = \; & (2hy - y^2)(\epsilon^2 \mathrm{We} h_{xxx} - h_x \cot\theta + \frac{2\mathrm{MaBi} y h_x}{1 + \mathrm{Bi}h)^2} + \\ & \mathrm{Re}h_t \left(\frac{y^3}{3} - hy \right) + \mathrm{Re}hh_x y \left(\frac{y^3}{6} - \frac{2h^3}{3} \right), \\ & p_1 = 0 \quad \text{and} \quad T_1 = \frac{\epsilon^n \mathrm{PeBi}^2 h_t}{6(1 + \mathrm{Bi}h)^2} \left(y^3 - \frac{(3 + \mathrm{Bi}h)}{(1 + \mathrm{Bi}h)} h^2 y \right) \\ & - \frac{\epsilon^n \mathrm{PeBi} h_x}{60(1 + \mathrm{Bi}h)^2} \left(3\mathrm{Bi} y^5 - 5(3\mathrm{Bi}h + 1) y^4 + \frac{(20 + 50\mathrm{Bi}h + 12\mathrm{Bi}^2 h^2}{(1 + \mathrm{Bi}h)} h^3 y \right). \end{aligned}$$

The $O(\epsilon^{2-n})$ terms of the equations are given by:

$$(4b)_{2-n}: \; u_{2_{yy}} = 2_{p_{1x}}$$
$$(5e)_{2-n}: \; u_2 = 0 \quad \text{on} \quad y = 0$$
$$(5b)_{2-n}: \; u_{2_y} = -2\mathrm{Ma}(T_{1_x} + h_x T_{1_y}) \quad \text{on} \quad y = h.$$

These yield

$$u_2 = \epsilon^n \mathrm{PeMaBi} y \left(\frac{(5 + 11\mathrm{Bi}h) h^4 h_x}{10(1 + \mathrm{Bi}h)^3} + \frac{2\mathrm{Bi}h^3 h_t}{3(1 + \mathrm{Bi}h)^3} \right)_x.$$

Now that the flow field has been determined at the desired level of approximation, we turn to the kinematic boundary condition for the free surface (5*d*), which can be written as $h_t + [\psi(h)]_x = 0$ where $\psi = \int_0^y u \mathrm{d}y$. This gives the evolution equation:

$$\begin{aligned} & h_t + 2h^2 h_x + \epsilon \left[-\frac{3}{10} \mathrm{Re} h^6 h_x - \frac{5}{12} \mathrm{Re} h^4 h_t - \frac{2}{3} h^3 h_x \cot\theta + \frac{\mathrm{MaBi} h^2 h_x}{(1 + \mathrm{Bi}h)^2} + \frac{2}{3} \epsilon^2 \mathrm{We} h^3 h_{xxx} \right]_x \\ & + \epsilon^2 \mathrm{PeMaBi} \left[h^2 \left(\frac{(5 + 11\mathrm{Bi}h) h^4 h_x}{20(1 + \mathrm{Bi}h)^3} + \frac{\mathrm{Bi} h^3 h_t}{3(1 + \mathrm{Bi}h)^3} \right)_x \right]_x = 0. \end{aligned}$$

As our expansion is truncated up to and including terms of $O(\epsilon^{2-n})$ we do not require any $O(\epsilon^2)$ terms at this level of approximation and so we can use the leading-order form of the above evolution equation, $h_t \sim -2h^2 h_x$, to remove h_t from the higher-order terms of the

evolution equation. The final equation is (9). Similarly, using the leading-order form of the evolution equation we can eliminate the explicit time derivative of h from u_1 and T_1 and u_2. This gives:

$$u_1 = (2hy - y^2)(\epsilon^2 \mathrm{We} h_{xxx} - h_x \cot\theta) - \frac{2\mathrm{MaBi} y h_x}{(1+\mathrm{Bi}h)^2} + \frac{1}{6}\mathrm{Re} h h_x y(8h^3 - 4hy^2 + y^3),$$
$$T_1 = \frac{\epsilon^n \mathrm{PeBi} h_x y^3}{(1+\mathrm{Bi}h)^2}\left(-\frac{y^2}{20} + \frac{(1+3\mathrm{Bi}h)_y}{12} - \frac{\mathrm{Bi}h^2}{3}\right) - \frac{\epsilon^n \mathrm{PeBi} h_x h^3 y}{30(1+\mathrm{Bi}h)^3}(10 - 5\mathrm{Bi}h - 4\mathrm{Bi}^2 h^2)$$

and

$$u_2 = \epsilon^n \mathrm{PeMaBi} y \left(\frac{(15 - 7\mathrm{Bi}h)h^4 h_x}{30(1+\mathrm{Bi}h)^3}\right)_x.$$

Appendix 2: Three-mode Galerkin model for the temperature field

The Galerkin projection in Section 5 truncated at $m = 3$ yields the following amplitude equations for τ, $A^{(2)}$ and $A^{(3)}$:

$$\begin{aligned}
0 \;=\;& \epsilon\mathrm{Pe} h\left(\frac{51 + 18\mathrm{Bi}h + 2\mathrm{Bi}^2h^2}{3}\tau_t + \frac{75 + 19\mathrm{Bi}h}{48}A^{(2)}_t + \frac{32 + 8\mathrm{Bi}h}{9}A^{(3)}_t\right)\\
&+ \epsilon\mathrm{Pe} q\left(\frac{2137 + 698\mathrm{Bi}h + 73\mathrm{Bi}^2h^2}{96}\tau_x + \frac{83 + 20\mathrm{Bi}h}{48}A^{(2)}_x + \frac{2107 + 501\mathrm{Bi}h}{528}A^{(3)}_x\right)\\
&- \epsilon\mathrm{Pe} q_x\left(\frac{454 + 119\mathrm{Bi}h}{192}\mathrm{Bi}h\tau + \frac{91 + 9\mathrm{Bi}h}{192}A^{(2)} + \frac{1985 + 247\mathrm{Bi}h}{3168}A^{(3)}\right)\\
&+ \epsilon\mathrm{Pe}\left(\frac{505 q_x}{192}(\tau - 1) + \frac{698 + 146\mathrm{Bi}h}{192}\mathrm{Bi}\tau q h_x - \frac{133 q_x \mathrm{Bi}h}{192}\right)\\
&+ \frac{7}{h}(6 + \mathrm{Bi}h)((1+\mathrm{Bi}h)\tau - 1) + (1+\mathrm{Bi}h)\frac{7A^{(2)} + 16A^{(3)}}{2h},
\end{aligned}$$

$$\begin{aligned}
0 \;=\;& \epsilon\mathrm{Pe}\left(h\left(\frac{75 + 19\mathrm{Bi}h}{48}\tau_t + \frac{19}{72}A^{(2)}_t + \frac{7}{12}A^{(3)}_t\right) + \frac{83 + 20\mathrm{Bi}h}{48}q\tau_x + \frac{91q}{352}A^{(2)}_x\right)\\
&+ \epsilon\mathrm{Pe}\left(\frac{51q}{88}A^{(3)}_x + \frac{31 q_x}{64}(\tau - 1) - \frac{17 q_x}{6336}A^{(2)} + \frac{43 q_x}{3168}A^{(3)} + \left(\frac{5}{12}q h_x - \frac{21}{64}h q_x\right)\mathrm{Bi}\tau\right)\\
&+ \frac{7}{2h}((1+\mathrm{Bi}h)\tau - 1) + \frac{6A^{(2)} + 13A^{(3)}}{2h},
\end{aligned}$$

$$\begin{aligned}
0 \;=\;& \epsilon\mathrm{Pe}\left(h\left(\frac{32 + 8\mathrm{Bi}h}{9}\tau_t + \frac{7}{12}A^{(2)}_t + \frac{128}{99}A^{(3)}_t\right) + \frac{2107 + 501\mathrm{Bi}h}{528}q\tau_x + \frac{51q}{88}A^{(2)}_x\right)\\
&+ \epsilon\mathrm{Pe}\left(\frac{745q}{572}A^{(3)}_x + \frac{1121 q_x}{1056}(\tau - 1) - \frac{5 q_x}{288}A^{(2)} + \frac{49 q_x}{10296}A^{(3)} + \frac{1002 q h_x - 793 h q_x}{1056}\mathrm{Bi}\tau\right)\\
&+ \frac{8}{h}((1+\mathrm{Bi}h)\tau - 1) + \frac{13}{2h}A^{(2)} + \frac{128}{9h}A^{(3)}.
\end{aligned}$$

The above three equations together with (17) and (21) constitute the TK1[3] model.

References

1. P.L. Kapitza and S.P. Kapitza, Wave flow of thin layers of a viscous fluid: III. Experimental study of undulatory flow conditions. *Zh. Eksp. Tear. Fiz.* 19 (1949) 105–120.
2. T.B. Benjamin, Wave formation in laminar flow down an inclined plane. *J. Fluid Mech.* 2 (1957) 554–74.
3. H.-C. Chang, Wave evolution on a falling film. *Annu. Rev. Fluid Mech.* 26 (1994) 103–136.
4. H.-C. Chang and E.A. Demekhin, *Complex Wave Dynamics on Thin Films*. New York: Elsevier (2002) 412 pp.
5. D.A. Goussis and R.E. Kelly, Surface waves and thermocapillary instabilities in a liquid film flow. *J. Fluid Mech.* 223 (1991) 24–45.
6. L. Scriven and C. Sternling, On cellular convection driven by surface-tension gradients: effects of mean surface tension and surface viscosity. *J. Fluid Mech.* 19 (1964) 321–340.
7. J. Pearson, On convective cells induced by surface tension. *J. Fluid Mech.* 4 (1958) 489–500.
8. S.W. Joo, S.H. Davis and S.G. Bankoff, Long-wave instabilities of heated falling films: two-dimensional theory of uniform layers. *J. Fluid Mech.* 230 (1991) 117–146.
9. S. Kalliadasis, E.A. Demekhin, C. Ruyer-Quil and M.G. Velarde, Thermocapillary instability and wave formation on a film falling down a uniformly heated plane. *J. Fluid Mech.* 492 (2003) 303–338.
10. S. Kalliadasis, A. Kiyashko and E.A. Demekhin, Marangoni instability of a thin liquid film heated from below by a local heat source. *J. Fluid Mech.* 475 (2003) 377–408.
11. V.Ya. Shkadov, Wave models in the flow of a thin layer of a viscous liquid under the action of gravity. *Izv. Akad. Nauk SSSR, Mekh. Zhidk. Gaza* 1 (1967) 43–50.
12. V.Ya. Shkadov, Theory of wave flow of a thin layer of a viscous liquid. *Izv. Akad. Nauk SSSR, Mekh. Zhidk. Gaza* 2 (1968) 20–25.
13. E.A. Demekhin and V.Ya. Shkadov, Three-dimensional waves in a liquid flowing down a wall. *Izv. Akad. Nauk SSSR, Mekh. Zhidk. Gaza* 5 (1984) 21–27.
14. C. Ruyer-Quil and P. Manneville, Further accuracy and convergence results of the modeling of flows down inclined planes by weighted residual approximations. *Phys. Fluids* 14 (2002) 170–183.
15. D. Gottlieb and S.A. Orszag, *Numerical Analysis of Spectral Methods: Theory and Applications.* Philadelphia: (SIAM (1977) 172 pp.
16. A. Oron, S.H. Davis and S.G. Bankoff, Long-scale evolution of thin liquid films. *Rev. Mod. Phys.* 69 (1997) 931–980.
17. O.A. Kabov, Formation of regular structures in a falling liquid film upon local heating. *Thermophys. Aeromech.* 5 (1998) 547–551.
18. E. Doedel, A. Champneys, T. Fairfrieve, Y. Kuznetsov, B. Sandstede and X. Wang, *Auto 97 Continuation and Bifurcation Software for Ordinary Differential Equations.* Montreal: Concordia University (1997) 157 pp.
19. C.M. Bender and S.A. Orszag, *Advanced Mathematical Methods for Scientists and Engineers*. New York: McGraw-Hill (1978) 593 pp.
20. T. Kawahara, Formation of saturated solitons in a nonlinear dispersive system with instability and dissipation. *Phys. Rev. Lett.* 51 (1983) 381–383.
21. A. Pumir, P. Manneville and Y. Pomeau, On solitary waves running down an inclined plane. *J. Fluid Mech.* 135 (1983) 27–50.
22. P.M.J. Trevelyan, S. Kalliadasis, J.H. Merkin and S.K. Scott, Dynamics of a reactive falling film in the presence of a first-order chemical reaction. *Phys. Fluids* 14 (2002) 2402–2421.
23. P.M.J. Trevelyan and S. Talliadasis, Dynamics of a reactive falling film at large Péclet numbers. I. Long-wave approximation. Phys. Fluids 16 (2004) 3191–3208.
24. P.M.J. Trevelyan and S. Kalliadasis, Dynamics of a reactive falling film at large Péclet numbers II. Nonlinear waves far from critically: Integral-binding larger approximation. Phys. Fluids 16 (2004) 3209–3226.